How the Waters off South Korea have Warmed over the Past Four Decades

by

Young-Heon Jo[1,*] L. C. Breaker[2], and Yu-Heng Tseng[3]

[1] College of Earth, Oceanography and Environment, University of Delaware, Newark, DE 19716

[2] Moss Landing Marine Laboratories, Moss Landing, CA 95039

[3] Department of Atmospheric Sciences, National Taiwan University, No. 1, Sec. 4, Roosevelt Rd. Taipei 10673, Taiwan

Revised and Resubmitted to
Continental Shelf Research

May 2010

[*] Corresponding author

Abstract

The East/Japan Sea (EJS) is located off the east coast of the Eurasian Continent and adjacent to the western North Pacific. Its response to various climatic influences is complex. The Korean Peninsula is surrounded by coastal waters that are strongly influenced by the EJS. In order to determine the magnitude of the warming that has occurred and to better understand how the waters off the Korean coast have warmed over the past four decades, we have analyzed the daily Sea Surface Temperature (SST) at three stations off the east coast of Korea for the 39-year period from 01-01-1966 to 12-31-2004. The stations are located approximately 66km apart at 37.8°N, 128.8°E (Station 3), 37°N, 129.5°E (Station 6), and 36°N, 129.7°E (Station 10). To examine these records, we employ several methods of analysis including Ensemble Empirical Mode Decomposition (EEMD), locally-weighted regression (LOESS), power spectrum analysis, and cumulative sums. In the case of EEMD we have also fitted linear trends to each mode to estmate the warming or cooling that has occurred for the time scales associated with each of the higher modes. With these tools, we address how the waters off the east coast of South Korea have warmed over the past four decades, ranging from seasonal to interdecadal time scales, and beyond.

Seasonal warming trends show that temperatures have increased by at least a factor of two higher in winter than in summer. The weakened Siberia High (SH) after circa 1980 through air-sea interaction during winter may significantly affect on seasonal warming of the coastal waters. SST on annual time scales has contributed to significant warming at all three stations. The contribution to warming on interannual time scales which includes warming and cooling from ENSO episodes, accounts for slight warming at station 3, but slight cooling at stations 6 and 10. On decadal time scales, the anomalies in SST (SSTAs) reveal maxima in temperature that occur in the mid-to-late 1970's, circa 1990, and circa 2000 at all three stations. These maxima coincide with major peaks in the North Pacific Gyre Oscillation (NPGO) with lags of 4-7 months with the NPGO leading in each case. The most significant warming appears in the long-term trends of SSTA at each station where the warming approaches +0.05°C/yr. The large-scale variation may result from an extension of the larger trend in ocean heat content in the North Pacific that is linked to the EJS through large-scale currents. Overall, sea surface temperature off the east coast of Korea has increased at rates that are far greater than reports from many other marginal seas around the globe.

Keywords: Global warming, Climate change, East/Japan Sea, HHT, etc

1. Introduction

The East Japan Sea (EJS) is a marginal sea located in the northwest Pacific surrounded by Korea, Japan, and Russia (Fig. 1). It is connected to adjacent seas by five shallow straits: the Korea/Tsushima Strait to the East China Sea, the Kanmon Strait and the Tsugaru Strait which connect to the Pacific Ocean, and the Soya Strait and the Tartar Strait which connect to the Okhotsk Sea. The mean depth of the EJS is 1,753 meters (m) and the deepest sea floor is 3,742 m below sea level.

The sea has three major basins: the Yamato Basin in the southeast; the Japan Basin in the north; and the Ulleung Basin in the southwest. The Japan Basin is the deepest basin, while the Ulleung Basin is the shallowest. While the eastern continental shelves are relatively wide, the western continental shelves are narrow, particularly along the Korean coast, averaging about 30 kilometers (km) in width.

There are four surface current systems in the EJS, the Tsushima Warm Current (TWC), the East Korean Warm Current (EKWC), North Korean Cold Current (NKCC), and the Liman Current. The NKCC and the EKWC meet along the east coast of Korea (Fig. 1). The warm saline water of the TWC passes through the Korea Strait, where the flow often bifurcates into western and eastern branches. According to Teague et al. (2002), the annual transport through the Korea/Tsushima Strait is 2.7Sv (Sv≡10^6 m^3s^{-1}). The eastern branch of the TWC flows northeastward along the Japanese coast (Yoon, 82) with some of its waters exiting through the Tsugaru Strait and the rest spreading further north into the NE Japan Basin. The western branch forms the EKWC and flows northward along the Korean coast (Seung, 1992). Then, the EKWC turns eastward between 37°N and 39°N, where it meets the NKCC which in turn is driven by the subpolar front (Seung and Kim, 1989; Seung, 1992). The NKCC originates in the Liman Current coming from the Tatar Strait. Some of the denser water in the NKCC intrudes along the coast below the surface as part of the EKWC. Thus, some subpolar water is transported south of the Korea Strait (Talley et al., 2006).

The seasonal wind stress plays an important role in the general circulation of the EJS, driving the anticyclonic subtropical circulation in the southern EJS, and cyclonic subarctic circulation in the northern EJS. The meridional location of the subpolar front varies significantly on a seasonal basis (Dorman et al., 2005), and the seasonal subpolar front separates the warm and the cold water masses of the EJS from the coast of Korea where they flow along the subpolar front (Fig. 1). Figs.2a and 2b show the summer and winter averaged surface pressure and current velocity vectors in the vicinity of the EJS from a fully three dimensional North Pacific Ocean model (resolution is 1/8° and 1/4° in the western and eastern Pacific, respectively). The simulation results show the flows to be strongly seasonal in nature. The summer averaged circulation represents the typical surface pattern from May-August (Fig. 2a) while the winter circulation corresponds to the period from November-February (Fig. 2b). The model reproduces many important features in the Asian Marginal Seas (AMS) and has been used in several related studies (e.g., Tseng et al., 2010a; 2010b). It is clear that the TWC can be seen as a branch of the warm Kuroshio as it enters the EJS. The Kuroshio is the dominant western boundary current and transports a significant amount of heat from low- to mid-latitudes. Intensive westward propagating eddies from the North Pacific commonly contribute to variations in the Kuroshio and the regional circulation in the AMS.

There are eleven water masses in the study area according to Talley et al. (2006). They defined the water masses based on several formation processes including subduction and open ocean convection. A number of studies devoted to the EJS were reported in a special issue of the *Journal of Oceanography* (Vol 19, No3, 2006). Only a small number of studies, however, have reported the impact of climate change in the EJS (e.g., Yasunari, 1990; Kang and Bak, 1993; An and Park, 1996; Oh, 1996; Minami et al., 1999; Hong et al., 2001; Park and Chu, 2006; Kang et al., 2005). The long term trend in temperature in the EJS has been analyzed in Minami et al. (1999), where they found a long-term variation in potential temperature (PT) and dissolved oxygen (DO) of the Japan Sea Proper Water (JSPW). For instance, there are large increases in PT and DO as much as 0.16±0.09 °C/century and 23.2±15.7μmol/century at 800m depth at the southeast EJS (Station P), respectively. As a result, water from JSPW into the deep layer has decreased for the last four decades. However, the study did not explain how or why the water in the EJS has warmed.

In this study, we used long time series of daily sea surface temperature (SST) at three locations along the east coast of Korea (Fig.1) to determine how these waters have warmed rather than those in the whole EHS. These records span the same 39- year period from January 1, 1966 through December 31 2004. To examine these records, we employ several methods of analysis including Ensenble Empirical Mode Decomposition (Wu and Huang, 2008), LOESS smoothing (Cleveland, 1979), power spectrum analysis, cumulative sums (Hawkins and Olwell, 1998), and the method of expanding means (Breaker and Flora, 2009). With these tools, we address the question of how the waters off the east coast of South Korea have warmed over the past four decades. We have organized this study based on time scales, starting with the shortest time scales, i.e., regime shifts (Section 4), followed by seasonal warming (Section 5), the annual cycle (Section 6), interannual variability (Section 7), decadal warming (Section 8), and, finally, long-term trends (Section 9).

2. Data and Data Processing

Since 1910, the Korean National Fisheries Research and Development Institute (NFRDI) has been collecting oceanographic and meteorological data at coastal stations along the Korean Peninsula (http:\\www.nfrda.re.kr). The network of observing sites includes a total of 40 coastal stations, but the periods of observations vary primarily due to the Korean War (1950-1953). Since 1981, the Korea Oceanographic Data Centre (KODC) has archived the data from most of these coastal monitoring stations.

The stations used in this study along the coast of Korea cover the southwestern region of the EJS, from 35°N to 38°N, and from 129°E to 132°E. For this study, we have selected three coastal stations: Station 3 (Juminjin) at 37.8°N, 128.8°E, Station 6 (Jukbyeon) at 37°N, 129.5°E, and Station 10 (Janggigap) at 36°N, 129.7°E (Fig. 1). The locations of these stations are approximately 66 km apart and are not influenced by freshwater discharge from rivers. With respect to data quality, there are 1716 (12%), 358 (2.5%), 268 (1.9%) missing observations out of a total of 14245 days (including leap days) at Stations 3, 6, and 10, respectively. The accuracy of the measurements is approximately ±0.1°C. Because most of the missing values were randomly spaced and not concentrated at just a few times, it has been a relatively simple matter to fill the gaps

using linear interpolation without compromising the overall quality of the data. Occasional outliers that exceeded the expected values by 5°C or greater were removed using a median filter.

After removing the leap days for computational convenience each record contains 14235 daily observations. Finally, for certain applications, the daily observations of SST have been weekly- or monthly-averaged. The mean, standard deviation (STD), variance, skewness, maximum, minimum, and range of SSTs are shown in Table 1. The variances in Table 1 are before and after applying the median filter, and show that the differences are relatively small.

The skewnesses in Table 1 are positive at each station indicating that the frequency distributions are not symmetric but skewed toward warmer temperatures. We have also calculated the running skewness to see if there were any long-term trends toward warmer temperatures. Although the variability in skewness was relatively high, there were no obvious long-term trends.

Fig. 3 shows two-way layouts of the daily SSTs by month along the vertical axis, and by year, along the horizontal axis. The figure reveals strong seasonal variations in SST with the highest temperature in August and September, and the lowest in February and March. Based on the locations of Stations 3, 6 and 10, we expected that significant differences between them might exist since their exposures to the NKCC and the EKWC coastal currents are somewhat different. To examine the inter-station differences, we calculated cross-correlations between the three stations, with, and without, pre-whitening. Pre-whitening removes the serial correlation from each time series. Long-range persistence or correlation is strong in these records because of the annual cycle. Pre-whitening effectively removes its influence, thus serving as a high-pass filter. The cross-correlation between Stations 3 and 10 is shown in Fig. 4. As expected, without pre-whitening, the dominance of the annual cycle is obvious in the upper trace (black). In this case, Station 3 lags Station 10 by approximately 2 days although whether or not this difference is statistically significant is open to question. Of greater interest in our view is the cross-correlation obtained after pre-whitening (shown by the blue trace). A small but statistically significant peak occurs at zero lag. This provides a measure of the information that is common to both locations. Because the peak occurs at zero lag, we can infer that propagating disturbances at least at the scales we can resolve with daily sampling are not a significant factor. However, as we shall see, there is information at much longer time scales contained in these residuals that will be examined later in the study. Similar results were obtained for the cross-correlations between stations 3 and 6, and 6 and 10. Although the lead-lag relationships with respect to the annual cycle were slightly different, again, we are not convinced that these differences are meaningful. However, the pre-whitened cross-correlations were almost identical in each case.

3. Ensemble Empirical Mode Decomposition

In order to examine to what extent the different time scales of SST variability contribute to warming (or cooling), we have decomposed the SSTs at each location into independent modes using Ensemble Empirical Mode Decomposition (EEMD). Each of these modes represents a certain range of zero-crossing periods or frequencies and ac-

counts for a certain fraction of the total variance. The variance by mode number is shown in the top panel of each figure. The modes are identified as C1 through C9, with the last mode referred to as the residual. The residual often contains information on any long-term trends in the data. In many cases, individual modes or selected mode groupings may provide physically meaningful interpretations. In such cases we may be able to relate a particular mode or mode grouping to a known physical process. The mathematical details of this procedure are given in the Appendix. The results of the EEMD decompositions are introduced here and shown in Figs. 5, 6 and 7.

In each case, the variance is greatest for mode C4, or modes C3 and C4, and represents the variance associated with the annual cycle. Modes C1 and C2 show high frequency variability in most cases, which is not of interest to us in this study. Although seasonal time scales are of interest, and their zero-crossing periods fall within modes C2 and C3, they are addressed outside the EEMD framework so that we could examine the different seasons separately. Modes C3 and C4 generally capture the variability associated with the annual cycle, modes C5 and C6 contains variability that occurs on interannual time scales, modes C7 and C8 contain variability generally associated with interdecadal time scales, and mode C9 and the residual contain information generally related to long-term trends. The contributions of each mode are discussed in the corresponding sections of the text.

4. The 1976-1977 Regime Shift

In order to examine the data on relatively short time scales, we first examined the EEMD results for the lowest modes, C1-C3, at each station. Specifically, we searched for indications of regime shifts, particulary the basin–wide event that occurred in late 1976 and early 1977. However, no indications of this event could be found in these modal time histories. As a result we have employed the method of cumulative sums to detect change points that may correspond to abrupt changes such as regime shifts. This method has been shown to be particulatly sentitive to detecting change points such as regime shifts in coastal observations of SST (Breaker, 2007; Breaker and Flora, 2009). Cumulative Sums (CUSUMs) represent the running total of the deviations of the first n observations from a mean based on the same interval (Page, 1954; Wetheril and Brown, 1991; Hawkins and Olwell, 1998; Breaker, 2007). The Cumulative Sums(CS) can be expressed as

$$\mathrm{CS}=\sum_{t=1}^{n}(x_t-\bar{x}) \qquad (1)$$

where x_t represents the nth observation, $\bar{x}$ is the mean of x_t from $t = 1$ to n, and CS is plotted versus time to produce the so-called CUSUM chart. Abrupt changes in the slope of the CUSUM often reflect change points, or, in our case, regime shifts. As a result of a regime change, coastal temperatures may increase or decrease, depending on the location. These events have time scales on the order of six months and may have a long-term impact on the mean state of the ocean.

The 1976-77 regime shift was a major event that affected most climatic and ecosystem indicators in the North Pacific basin and has been documented extensively. Breaker (2007) and Breaker and Flora (2009) used daily and weekly SSTs from single locations off the coasts of California and Hawaii to examine the 1976-77 regime shift and other regime shifts in detail. CUSUMs were calculated from the daily and weekly time

series to detect and localize these events. Breaker and Flora (2009) were able to detect and localize the 1976-77 event off southern California and Hawaii and found that SSTs increased by up to +1°C off Southern California, and by up to +0.5°C off Oahu, Hawaii.

Because the 1976-77 regime shift was reported to be basin-wide in its extent (e.g., Bakun, 2004), we have examined the daily observations from Stations 3, 6, and 10 to determine if it could be detected off the coast of South Korea. CUSUMs were calculated for all 3 stations, and the results are shown in Fig. 8, together with the CUSUMs for Scripps Pier, off southern California (8a), and Koko Head, off Oahu, Hawaii (8b). The CUSUMs for Stations 3, 6, and 10 are shown in blue, green, and red, respectively. Because the slopes are all negative they imply that a decrease in temperature occurred. If we compare the approximate mid-points of this event in the CUSUMs at Scripps Pier and off the coast of South Korea, it appears that its arrival off the coast of South Korea was delayed by several months, suggesting that this event did not occur simultaneously throughout the North Pacific basin.

To estimate the impact of the 1976-77 regime shift, we have also calculated what Breaker and Flora (2009) refer to as an expanding mean diagram (Fig. 8d) for Station 6. We chose to display the results of the expanding means for Station 6 for two reasons. First, it was slightly easier to interpret the differences between the backward and forward directions from t_0 than for the other two stations. Second, the differences in each case were generally similar and so there was no compelling reason to show the results for all three stations. Starting at the mid-point of the regime shift, mean temperatures are calculated moving away from the mid-point in the forward and reverse directions, one day at a time, until the mean values extend out to several years. The plots tend to stabilize after roughly the first year and often significant differences are found. In this case, after year one, we observe slight decreases in temperature at each station although it is most apparent at Station 10 (not shown). At Station 3, by the end of year two, the temperatures were almost the same, and thus show little long-term impact. The changes that do occur tend to reflect decreases in temperature, and, as a result, they are consistent with the CUSUMs which clearly indicate decreases in temperature due to the negative slopes. We find it interesting that although the long-term trends at each station are strongly positive over the entire record, the changes that occurred during the 1976-77 regime shift, if anything, served to decrease temperatures over the period where their impact could be detected.

In response to regime shifts, several studies have reported that the impact of climatic regime shifts was significant in the EJS with respect to marine ecosystem and fisheries resources. Zhang et al. (2000) analyzed the impact of the 1976 regime shift on Korean waters and found that this event increased the mixed layer depth (MLD), and contributed to biological changes in the ecosystems off Korea where the influence of the 1976 regime shift was evident in a decreased biomass and production of saury, but an increase in biomass and production of sardines and filefish.

5. Warming on Seasonal Time Scales

In order to examine possible seasonal influences on the warming process we have calculated monthly means for each station and then created separate sequences for each month, producing 12 time series, each containing 39 monthly val-

ues. Although the monthly values are widely scattered we have fitted linear trends to each time series using the method of least squares. To provide a measure of the goodness-of-fit to the linear trends, the standard deviations for each month and station were also calculated. They are given in Table 2. What these deviations show is a weak tendency for the scatter about the monthly means to decrease slightly between January and December.

Next, the slopes were extracted from each linear trend and the results plotted by month and station in Fig. 9. Smoothed versions of the plots of the monthly slopes are also included as well as the slopes for the entire records. The slopes for the entire record range from +0.066°C/year in February to +0.023°C/year in July for Station 3, from +0.065°C/year in May to +0.045°C/year in September for Station 6, and from +0.066°C/year in February to +0.023°C/year in July for Station 10. These rates of increasing temperature are relatively large, implying long-term increases of up to ~6.5°C during the winter season and up to ~2.3°C during the summer season over 100 years.

Although we expected the largest slopes during the summer when seasonal heating is a maximum, the tendency is for the smallest slopes to occur during the summer and the largest slopes to occur during the winter, especially for stations 3 and 10. Station 6 is located in the subpolar front and is influenced by both the NKCC and the EKWC (Fig. 1), which may help to explain the different seasonal warming rates in this case.

For comparison, Balling et al. (1998) estimated winter and summer warming rates on global scales over the period from 1946 to 1995. They found that warming is greatest at higher latitudes in the Northern Hemisphere, particularly in the low-sun season, rather than in the high-sun season. Specifically, they found a warming rate of +0.08°C/decade for the winter season and +0.05°C/decade for the summer season. On regional scales, Belkin (2000) reported changes in SST in four different regional seas between 1982 and 2006. He found warming rates for the Baltic Sea of +0.054°C/yr, for the North Sea, +0.0524°C/yr, for the East China Sea, +0.0488°C/yr and for the EJS, +0.0436°C/yr. During the same period, the SST warming rate for our study was approximately +0.048°C/yr. Although we originally thought that the warming rates we observed off the Korean coast were relatively high, we find from Belkin's results that this may not be the case.

6. The Annual Cycle

In order to examine certain aspects of the annual cycle we have first calculated the Mean Annual Cycle (MAC) by calculating the mean value for each day of the year taken over the number of years in the record. The MACs for Stations 3 (blue), 6 (green), and 10 (red) are shown in Fig. 10a. Slightly smoothed versions are also shown. A period during July has been highlighted in green and is shown in expanded form in Fig. 10b. The slightly reduced temperatures compared to the smoothed versions are due to upwelling which is known to occur along the coast due to the seasonal winds which become upwelling-favorable at this time of year (Lee, 1978; Lee, 1983).

The annual cycle is the dominant feature in the record at each station. Compared to the variance of the entire record, the variance of the MAC is 90.5% of the total va-

riance at Station 3, 86.7% of the total variance at Station 6, and 89.8% of the total variance at Station 10. In Table 3, we include some basic statistics associated with the MAC at each location. The mean values for the MAC are almost identical to the global means for the original data. Not surprisingly, the maximums are decreased, the minimums increased, and thus the range is decreased significantly when we compare these values with the corresponding values for the original data in Table 4.

In order to determine the contribution of different time scales to warming and cooling, we have drawn upon the EEMD analyses shown in Figs. 5, 6 and 7. The results of the EEMD analyses form the basis for Figs.11a and 11b, which will be referred to frequently. First, linear slopes have been fitted to the data for each station and are shown as horizontal dashed lines. In addition, the solid lines show the linear slopes when selected modes were withheld in order to estimate the contribution of each mode to the warming process. Departures from the original slope indicate warming when they lie below the horizontal line, and cooling, when they lie above. Approximate confidence limits associated with the slopes for each station have also been included. Following Emery and Thomson (2004), we calculated the de-correlation time scales from the autocorrelation functions (ACFs) and then estimated the degrees-of-freedom, N^*, from $N^*=N/\tau$, where N is the original number of observations and τ is the de-correlation time scale, taken as the time required for the ACF to decay to 1/e (0.368). Then we applied a standard t-test (e.g., Huntsberger, 1965) to determine the 95% confidence limits. Because N^* is far smaller than N, the associated confidence limits are relatively wide and overlap extensively for all three stations, indicating that the differences in the slopes are often not statistically significant. However, none of the lower confidence limits cross zero which indicates that all of the slopes are significantly greater than zero, at the 95% significance level.

The modes C3 and C4 correspond to the annual cycle and show that they do contribute to higher SSTs (Fig. 11a). Specifically, as shown in Fig. 11a, these modes contribute to significant warming at stations 3 (+0.047°C/yr), 6 (+0.05°C/yr), and 10 (+0.034°C/yr). That the warming is similar at each location is consistent with the possibility of an atmospheric contribution to the warming process on this time scale. We also note that the seasonal warming trends shown in Fig. 9 indicate that this warming is greatest during the winter.

Because of the dominance of the annual cycle, at this point we have removed the MAC from the data in order to examine interannual, decadal and longer changes in temperature with greater clarity. We note that although this procedure removes most of the variance associated with the annual cycle it does not remove all of it since the amplitude of the annual cycle in most cases varies with time. However, this is the procedure that is most often used in correcting the data for its influence. For station 3, the variance after removing the MAC is reduced from 33.0 to 2.9 (a 91% reduction), for station 6, from 21.8 to 2.54 (an 88.3% reduction), and for station 10, from 27.9 to 2.39 (a 91.4% reduction) (also see Table 4).

7. Influence of El Nino and La Nina Episodes

Now we examine the variability in SST on interannual time scales. By removing the MAC, we can examine the residuals which are often referred to as Sea Surface Temperature Anomalies, or SSTAs. ENSO events including both El Nino and La Nina epi-

sodes occur on interannual time scales. According to Hong et al. (2001), SSTAs in the EJS are closely related to ENSO events. Their results indicate (1) that the summer in the year in which El Nino events develop tends to be colder than in the year prior to the event, whereas the winter tends to be warmer, and (2) that during La Nina events these patterns are reversed. In order to identify the timing and magnitude of ENSO events we have employed the Multivariate ENSO Index (MEI) (http://www.cdc.noaa.gov/people/klaus.wolter/MEI/), where strongly positive values that persist for up to a year or longer represent El Nino events, and negative values that persist for up to a year or longer represent La Nina events (Fig. 12a). The MEI shows that La Ninas tended to dominate prior to the mid-1970s, at about the time of the 1976-77 regime shift, whereas El Ninos tend to dominate following this period.

We have examined the SSTAs at all three stations to see if we could detect patterns similar to those observed by Hong et al. (2001) along the coast of Korea. The results are shown in Fig. 12. We observe decreases in SSTA of almost 2°C, up to a year, prior to the 1982-83, 1986-87, and 1997-98 El Nino events, as indicated by the vertical yellow dashed lines.

We see similar decreases in SSTA during the 1992-93 El Nino but it is not clear from the MEI when this event actually started. We do not see any clear relationship between the SSTAs and La Nina events. Overall, we do not observe the same relationships as those observed by Hong et al. (2001). The reasons are as follows. Stations 3, 6, and 10 are directly exposed to the influence of the NKCC and the EKWC coastal currents, and not to the open waters of the EJS. Figs 1, 2a and 2b show that the circulation off the coast of South Korea is quite distinct from the circulation further offshore in the EJS. Consequently, it is not surprising, and perhaps to be expected, that our results differ from those of Hong et al. (2001).

However, these results do show what might be called pre-cursors to the major El Nino episodes (e.g., the 1982-83 event). That we observe "pre-cursor" events, i.e., relatively large decreases in temperature, prior to the major El Ninos since 1980, may be significant and potentially useful in a predictive sense. These cooling events before major ENSOs could be associated with the commonly recognized "Seasonal Footprinting Mechanism" (SFM) at mid-latitudes that often occurs prior to ENSO events (Vimont et al., 2003). The SFM suggests that Northern Hemisphere wintertime sea level pressure variability over the extratropics initiates an SST footprint onto the ocean via changes in the net surface heat flux. The North Pacific Oscillation (NPO), like sea level pressure patterns, may be related to the cool pre-cursor events observed in the EJS. Further study is required to investigate the pre-cursor mechanisms.

Next, we conducted a cross-correlation analysis between the MEI and the SSTAs at each station.[1] The results indicate weak but consistent correlations between the MEI and all three stations, with maximum negative correlations occurring at lags of 3-4 months and slightly larger positive correlations occurring at lags of about 11-13 months, with the MEI leading in these cases. In most cases, the correlations were not statistically significant at the 95% level of confidence. However, at Station 10, the largest maximum correlation occurred at a lag of approximately one year, with Station 10 leading the MEI, generally consistent with our previous observations from Fig.12. We conclude that the

[1] Both pre-whitened and non-pre-whitened cross-correlations were calculated and the results were generally similar for both.

variability associated with the SSTAs on interannual time scales is not completely independent of that associated with ENSO events, and although the relationships are weak, they may still be meaningful.

From our EEMD decomposition, the zero-crossing periods associated with modes C5 and C6 correspond to interannual time scales and so include ENSO-related variability. In order to examine whether ENSO events contribute to long-term warming or cooling, as with the lower modes, we computed the trends with and without the ENSO-related modes (Figs. 11a and 11b). While the ENSO events appear to contribute to slight cooling at stations 6 and 10, they apparently contribute to warming at station 3. More specifically, the trends in SST without the ENSO signals (C5 and C6) showed that they contribute to warming of +0.006°C/yr at Station 3, cooling of -0.011°C/yr at Station 6, and cooling of -0.01°C/yr at Station 10 as shown in Fig 11a. The corresponding warming or cooling associated with these trends in SST is 10%, -3%, and -11%, respectively (Fig. 11b). Finally, the associated confidence limits are relatively wide and overlap extensively for all three stations, indicating that the differences in the slopes may not be statistically significant and that the differences with and without modes C5 and C6 may not be statistically significant.

In addition to regime shifts, ENSO events also affect marine ecosystem and fisheries in the EJS. Kim and Kang (2000) analyzed ecological variations due to El Ninos off the south coast of Korea using the Southern Oscillation Index (SOI) and SST as indicators. The SOI and SST in December were highly correlated and the variability in anchovy and mackerel catch was associated with El Nino episodes because of changes in the ecosystems in December.

8. Decadal Warming

Next we consider variability in SSTA on decadal time scales. We consider a major contributor to the decadal warming, which is due to thermal advection in the EKWC resulting from sea level changes in the North Pacific through changes in the Kuroshio Current System. For the relations between SSTA off the east coast of Korea and the North Pacific current system, we consider the North Pacific Gyre Oscillation (NPGO)[2], which is a climate pattern that emerges as the second dominant mode of sea surface height variability in the Northeast Pacific (Di Lorenzo et al., 2008). Variations in the NPGO may reflect changes in the intensity of the North Pacific gyre circulation. The study showed that fluctuations in the NPGO are driven by regional and basin-scale variations and horizontal advection in the North Pacific.

In order to examine the relation between SSTA and the NPGO, we performed a cross-correlation analysis and found that the lags vary from 4-7 months, with the NPGO leading in each case. The dominant peaks in the NPGO are approximately 12 years apart (peaks at 1976, 1987, and 2000), with the major peaks in the SSTA being closely aligned, taking into account the lag relationship. The peaks are most likely related to the decadal scale oscillations that are reflected in the NPGO index and that have so often been observed and reported in the EJS (e.g., Gordon and Giulivi, 2004). From the EEMD analyses we see that mode C7 captures the time scales associated with decadal scale varia-

[2] http://www.ocean3d.org/npgo

tions as shown in Figs. 5, 6, and 7 for stations 3, 6, and 10, respectively (Fig. 13a). We then compared mode C7 from an EEMD analysis of the NPGO index time series with mode C7 for the three stations and find a high degree of similarity (Fig. 13b), consistent with our interpretation of the results shown in Fig. 13a. These quasi-decadal maxima in SSTA and the NPGO are also most likely related to the 10-15 year ENSO modulation cycle that has been identified and discussed in detail (or called El Nino Modoki) in recent years (e.g., Yeh and Kirtman, 2005; Sun and Yu, 2009). According to Di Lorenzo et al. (2009), the decadal dynamics of the Pacific Decadal Oscillation (PDO) and the NPGO are linked through their relationship to ENSO events, and the second dominant NPGO mode (affected by the North Pacific Oscillation) is well captured from our decadal warming cycle. This indicates the extensive impacts of NPGO and its related circulation process.

9. Long-Term Warming Trends

The impact of warming associated with the long-term trends from the residual mode (R) of the EEMD decomposition is shown in Fig. 11a. The long-term trends for residual mode at each station clearly are the largest contributors to the warming process (Fig. 11b) after 1961. Their impacts are far greater than that from any of the lower modes. Fig. 14 shows the linear trends, the LOESS smoothings, and the residuals from the EEMD decomposition plotted together for each station. From the long-term trends (black) and the EEMD residuals (red), we see that SSTAs have increased by as much as 1.5°C to 2.0°C from 1966 to 2004, and that the rate of increase approaches +0.05°C/year. The LOESS smoothings in addition show the previously discussed major peaks in the mid-1970's, circa 1990, and circa 2000, that are superimposed on the long-term warming trends. The warming trends are similar at each station suggesting that the process or processes responsible for this warming are not local in nature but most likely affect the entire region (e.g., Levitus et al., 2000; 2005).

10. Discussion

The EJS is often regarded as a subset of the North Pacific Ocean and, as such, is used to assess the influence of global climate change. Since the EJS is located at mid-latitudes off the east coast of the Eurasian Continent and also adjacent to the Western Pacific, its climate-related changes are due to many factors. According to the Intergovernmental Panel on Climate Change (IPCC), the long-term rate of increase in global surface temperature is approximately +0.005°C/year (IPCC, 2007), which is far smaller than that for the EJS which has been estimated to be +0.017°C/yr (Belkin, 2009). This study shows that the warming trend off the east coast of South Korea approaches +0.05°C/yr which is almost three times higher than the warming trend for the EJS per se. As a result, it becomes clear that local effects off the east coast of Korea such as the advection of warmer waters along the Korean coast from the EKWC must be taken into account in order to explain why these warming rates differ so widely.

In order to address how the waters off the east coast of Korea warmed over the past four decades (1966 to 2004), we decomposed the data into a sequence of independent modes using EEMD so that we could examine the warming process on different time

scales. We see that warming has occurred on annual, interannual, and interdecadal time scales but that the greatest warming has occurred on time scales that are of the order of the record length, or longer. We find this result slightly at odds with the previous result that far greater warming has occurred along the coast of South Korea than over the EJS itself, since warming at longer time scales usually implies that warming has taken place over larger spatial scales as well. Fig. 15 shows the seasonal differences in SST over the 25-year period from 2007 to 1982. It clearly reveals significant warming the EJS in winter rather than in the summer, especially along the northwestern boundary of the EJS.

Our results also show that there are higher warming rates during the winter season than summer for all three stations. These seasonal changes are significant and are consistent with the results of Ross et al. (1996), who found warming over Siberia related to a weaker Siberian High (SH) in winter leading to milder winters over the East Asia region including the waters off the east coast of South Korea. Youn (2005) showed that the SH air mass has warmed significantly during the winter period over the past several decades, which may be an important contributing factor to the seasonal warming that we have observed along the coast of South Korea. The study illustrated the relation between the weakening of the SH and decreasing northerly winds during the winter and found the warming trend in air temperature is +1.5°C for 100 years around the Korean peninsula.

The influence of ENSO events as they affect the variability in SST in the EJS was examined. After extracting ENSO events from the SSTAs, our results show that while SST increased at station 3 (+14%), SST decreased at stations 6 (-26%) and 10 (-30%). The reason for the differences between stations is as follows. Extreme phases of ENSO events modulate the general circulation in the marginal sea through global air-sea interactions (Park and Oh, 2000). Since SST is primarily determined by these circulation systems, different aspects of ENSO influence arise from the subpolar front associated with the general circulation pattern in the region. The subpolar front is zonal in orientation and crosses the EJS at about 37-39°N (Fig. 1). This front divides the sea into subtropical and subpolar regimes. While the subtropical circulation, south of the subpolar front, is somewhat anticyclonic, the subpolar circulation, north of the subpolar front, is cyclonic. As a result, stations 6 and 10 are under the influence of the subtropical circulation, and the EKWC, while station 3 is primarily under the influence of the subpolar circulation and the NKCC.

The Kuroshio's main tributary, the TWC, enters the EJS through the Korea/Tsushima Strait and flows across the EJS. Warm water transported by this current depends on SSH differences between the Northwest Pacific and the EJS (Figs. 2a and 2b). The station locations employed in this study are well suited to detect signals associated with the Kuroshio. The monthly mean SSTA, the NPGO, and EEMD C7 all reveal decadal scale variations, which contribute significantly to the warming process (Fig. 11b). Since the NPGO is locally forced by surface wind variability associated with NPO, it can be seen as the oceanic expression of NPO, which characterizes the high sea level pressure over Hawaii and low pressure in the Gulf of Alaska. The oceanic sea level anomalies forced by the NPO could trigger oceanic adjustment through westward propagating Rossby waves, which can reach the North Pacific western boundary and modulate the decadal variation of the Kuroshio Current System (Tseng et al., 2010b). Thus, the results in the observed decadal signals in this study link to the Kuroshio. These results are also consistent with the possible pre-cursor signals found prior to ENSO episodes (see section

7). Casey and Adamec (2002) studied the relationship between SST and SSH variability over the North Pacific and showed that some of the Kuroshio transport-related changes are due to variations in the subtropical Pacific SSH. Han and Kang (2003) estimated how much heat is transported into the EJS through the Korea Strait. Using historical surface current data, from 1999 to 1993 (Japan Oceanographic Data Center), they estimated heat supplied by the current (HSC) in the EJS. The results showed that heat transport associated with the HSC was large in the northwest EJS, and small in the southeast EJS, suggesting that the warm current is restricted primarily to the surface layer around the northeast EJS, and extends deeper in the southeast EJS. Thus, heat transport from the north Pacific may be a significant factor that contributes to the thermal regime in the EJS.

Thus, our results are consistent with large changes in heat content observed in other Asian marginal seas through transport by advection (Tseng et al., 2010c). These large-scale decadal variations may be an extension of the larger trend in ocean heat content in the Western Pacific shown in earlier studies (Levitus et al., 2005; Ishii et al., 2006; Tseng et al., 2010c), reflecting the regional response to interannual/decadal climate variability. This argument is supported by the consistency and high correlation with 4-7 month lags between the SSTA and the NPGO, which is not surprising and reflects the advection speeds associated with the basin-scale current transport (e.g. through the Korean Strait in Fig. 1) as discussed in section 8.

11. Summary and Conclusions

We analyzed sea surface temperatures measured along the east coast of South Korea from 1966 to 2004 to quantify the magnitude of warming and to understand how the waters have warmed based on different time scales, starting with the shortest time scales which correspond to regime shifts, followed by seasonal warming, the annual cycle, interannual variability, decadal warming, and long-term trends. The results of this study show that warming has occurred on different times scales and by examining these time scales separately we have learned more about the processes that are been responsible for the observed warming.

A number of conclusions can be drawn from this study. First, sea surface temperatures increase more in winter than in the summer season. The winter circulation and water mass formation in the EJS are thought to be strongly driven by cold winds from the Siberian High. Second, the influence of ENSO events to warming/cooling trends depends on location along the coast of Korea. Although ENSO events contribute to warming at station 3, they contribute to cooling at stations 6 and 10. This may be traced to different water masses that are separated by the subarctic front (station 3) and the subtropical front (stations 6 and 10). Third, the decadal warming in the EJS is related to warm water that is advected from the Northwest Pacific as illustrated through the NPGO. This shows that the EJS should belong to a part of the Western Pacific circulation system rather than to an independent basin. Finally, according to our observed long-term warming trends, they are significantly larger than the global warming trend reported by the IPCC. SST in the is case) has increased by up to eight times the global average (~+0.041°C/yr versus ~+0.005°C/yr).

Acknowledgements

This research was supported partially by NASA through its Physical Oceanography and EPSCoR programs and by NOAA Sea Grant program.

Appendix

Hilbert Spectral Analysis/Empirical Mode Decomposition (HSA/EMD) is a relatively new empirical technique for analyzing non-stationary and nonlinear time series that includes HSA and EMD. The method was introduced by Huang et al. (1998), and further described in Huang and Shen (2005a), and Huang and Attoh-Okine (2005a). Based on EMD, the data are initially decomposed into a set of Intrinsic Mode Function (IMF) components. Local maxima and minima are identified in the record and envelopes are formed by fitting cubic splines to the extreme values. The differences between the envelope and the mean provide an estimate of the first IMF component. These steps are repeated to obtain improved estimates of the first IMF. The process, called sifting, extracts the essential scales from the data. According to Huang et al.(1998), an IMF represents a simple oscillatory mode, and, in general, has variable amplitude and frequency expressed as functions of time.

Once the first IMF, imf_1, has been obtained, based on the stopping criterion adopted, it is subtracted from the original data, $x(t)$, producing a set of residuals, r_1, which can be expressed as

$$x(t) - imf_1 = r_1 . \qquad \text{(A1)}$$

The residuals, r_1, are then subjected to the same process, yielding the second IMF, imf_2, as

$$r_2 = r_1 - imf_2 , \qquad \text{(A2)}$$

and so on, until a final residual is obtained that often corresponds to a long-term trend in the data. Because the IMF components are essentially independent and thus can be linearly combined, we can reconstruct the original record, $x(t)$, according to

$$x(t) = \sum_{i=1}^{n} imf_i + r_n \qquad \text{(A3)}$$

where n represents the total number of IMFs. According to Huang (2005a), the IMF components are often physically meaningful and so can provide insight into the processes involved.

One of the major problems with conventional EMD is the frequent appearance of mode mixing which can produce signals of disparate scales residing in the same IMF component. In order to overcome this problem, Wu and Huang (2008) introduced a newer version of EMD called Ensemble Empirical Mode Decomposition (EEMD) that produces improved IMF components calculated as the mean of an ensemble of trials, each consisting of the signal plus white noise of finite amplitude. The i^{th} realization of the simulated observations can be expressed as

$$x_i(t) = x(t) + w_i(t) \qquad \text{(A4)}$$

where, $x(t)$ is the original signal, i.e., imf, $w_i(t)$ represents the i^{th} realization of the white noise process, and $x_i(t)$ is their sum. Extensive testing has shown that the quality of the decompositions is improved using this approach (Wu and Huang, 2008).

References

An, J.B., Park, H.S., 1996. An atmospheric response to SST anomaly in the tropical Pacific using GCM with OSU two-layer. *J. Korean Meteorol. Soc.,* 32/3, 389-399.

Bakun, A., 2004. Regime shifts. In: A.R. Robinson, J. McCarthy and B.J. Rothchild, Editors, The Sea 13, Wiley, New York (2004), pp. 971–1018.

Balling, R.C., Michaels P., Knappenberger P.C., 1988. Analysis of winter and summer warming rates in gridded temperature time series. *Climate Res.,* 9,175-181.

Belkin,I.M., 2009. Rapid warming of large marine ecocystems. *Prog. Oceaogr.*, 81, 207-213.

Breaker, L.C., 2007. A closer look at regime shifts based on coastal observations along the eastern boundary of the North Pacific. *Cont. Shelf Res.*, 27, 2250-2277.

Breaker, L.C., Flora, S.J., 2009. Expressions of 1976–1977 and 1988–1989 Regime Shifts in Sea-Surface Temperature off Southern California and Hawaii. *Pacific Sci.,* 63(1):39-60.

Casey, K.S., Adamec, D., 2002. Sea surface temperature and sea surface height variability in the North Pacific Ocean from 1993-1996. *J.Geiphys.Res.,* 107, 10.1029/2001JC001060.

Cleveland, W.S., 1979. Robust locally weighted regression and smoothing scatter plots. *J. AM. Stat. Assoc.,* 74, 829–836.

Di Lorenzo, E., Schneider, N., Cobb, K.M., Franks, P.J.S., Chhak, K., Miller, A.J. , McWilliams, J.C., Bograd, S.J., Arango, H., Curchitser, E., Powell, T.M., 2008. North Pacific Gyre Oscillation links ocean climate and ecosystem change, *J. Geophys. Res. Lett.*, 35, L08607, doi:10.1029/2007GL032838.

Di Lorenzo, E., Schneider, N., Cobb, K.M., Furtado, J.C. , Alexander, M.A. Anderson, B. , 2009. ENSO and the North Pacific Gyre Oscillation: an integrated view of Pacific Decadal dynamics. Submitted to *J.Geophys. Res. Lett.*

Dorman, C.E., Beardsley, R.C., Limeburner, R., Varlamov, S.M., Caruso, M., Dashko, N.A., 2005. Summer atmospheric conditions over the Japan/East Sea. *Deep-Sea Res.* II, 52. 1393-1420.

Emery, W.J., Thomson, R.E., 1997. Data analysis methods in physical oceanography. Gray Publication, Pregamon, Kent, Great Britain.

Gordon, A. L., Giulivi, C.F., 2004. Pacific decadal oscillation and sea level in the Japan/East sea. *Deep Sea Res.,* 51. 653-663.

Han, I.S., Kang, Y.Q., 2003. Supply of heat by Tsushima Warm Current in the east Sea (Japan Sea). *J. Oceanogr.,* 59, 317-323.

Hawkins, D.M. Olwell, D.H.,1998. Cumulative Sum Charts and Charting for Quality Improvement, Springer, New York.

Hong, C.-H., Cho, K.D., Kim, H.-J., 2001. The relationship between ENSO events and sea surface temperature in the East (Japan) Sea, *Prog. Oceaogr.,* 49, 21-40.

Huang, N.E. and others., 1998. The empirical mode decomposition and the Hilbert spectrum for nonlinear and non-stationary time series analysis. *P. R. Soc. London*. A 454, 903- 995.

Huang, N.E. Shen, S.S.O., 2005a. Introduction to the Hilbert-Huang Transform and its related mathematical problems, p. 1-24. In N.E. Huang and S. S. P Shen (eds.),

Hilbert-Huang Transform and its applications, Interdisciplinary Mathematical Sciences - Vol. 5. World Scientific, New Jersey.

Huang, N.E., Attoh-Okine, N.O., 2005b. Introduction to the Hilbert-Huang Transform and some recent developments, p. 1-24. In N.E. Huang and N.O. Attoh-Okine (eds.), Hilbert-Huang Transform in Engineering. Taylor & Francis, Boca Raton.

Huntsberger, D.V., 1965. Elements of Statistical Inference. Allyn and Bacon, Inc., Boston.

Ishii M., Kimoto M., Sakamoto ,K., Iwasaki, S.-I., 2006. Steric Sea Level Changes Estimated from Historical Ocean Subsurface Temperature and Salinity Analyses. *J. Oceanogr.,* 62, 155-170.

Intergovernmental Panel on Climate Change (IPCC). 2007. Summary for Policymakers: Climate Change 2007: The Physical Science Basis. Contribution of Working Group I to the Fourth Assessment Report of the Intergovernmental Panel on Climate Change.

Kang, S. K., Cherniawsky, J. Y., Foreman, M. G. G., Min, H. S., Kim, C.-H., Kang, H.-W., 2005. Patterns of recent sea level rise in the East/Japan Sea from satellite altimetry and in situ data, *J. Geophys. Res.*, 110*,* C07002, doi:10.1029/2004JC002565.

Kang, I.S., Bak, H.J.,1993. A long-term prediction of monthly mean air temperature in Korea during winter. *J. Korean Meteorol. Soc.,* 29. 253-262.

Kim S., Kang S., 2000.Ecological variations and El Nino effects off the southern coast of the Korean peninsula during the last three decades, *Fish. Oceanogr*., 9(3): 239-247.

Lee, J.C.,1983. Variations of sea level and sea surface temperaure associated with wind-induced upwelling in the southeast coast of Korea in summer. *J. Korean Oceanogr. Soc.,* 18, 149-160.

Lee, K.B.,1978. Study on the coastal cold water near Ulsan. *J. Korean Meteorol. Soc.,* 13,5-10.

Levitus, S., Antonov, J. I., Boyer, T. P., Stephens, C., 2000. Warming of the World Ocean, *Science,* 287**,** 2225-2229.

Levitus, S., Antonov, J., Boyer, T.P., 2005. Warming of the world ocean, 1955–2003. *J. Geophys. Res. Lett.*, 32, L02604, doi:10.1029/2004GL021592.

Minami, H., Kano, Y., Ogawa, K., 1999. long-term variations of potential temperature and dissolved Oxygen of the Japan Sea Proper Water. *J. Oceanogr.*, 55, 197-205.

Oh, J.S.,1996. A study of Asian Monsson in summer during El Nino in 1987 and La Nina in 1988 using METRI/YONU GCM. *J.Korean Meteorol. Soc.,* 32, 111-129.

Page, E.S. 1954. Continuous inspection schemes, *Biometrika*, 41, 100–115.

Park, S., Chu, P.C., 2006. Interannual SST variability in the Japan/East Sea and relationship with environmental conditions. *J. Oceanogr.*, 62, 115-132.

Park, W.S., Oh, I.S., 2000. Interannual and interdecadal variations of sea surface temperature in the East Asian Marginal Sea. *Prog. Oceanogr.,* 47, 191-204.

Ross R.J., Otterrnan, J., Starr, D.O.C., Eliott, W.P., Angell, J.K., Susskind, J., 1996. Regional trends of surface and tropospheric temperature and evening-morning temperature difference in northern latitudes- 1973-93. *J.Geophys. Res. Lett.,* 23, 3179-3182.

Seung Y, H.,1992. A simple model for separation of East Korean Warm Current and formation of North Korean Cold Current. *J. Korean Oceanogr. Soc.*, *27*, 189-196.

Seung, Y. H., Kim, K.,1989. On the possible role of local thermal forcing on the Japan Sea circulation. *J. Korean Oceanogr. Soc.*, 24, 29-38.

Sun, F., Yu, J.-Y., 2009: A 10-15year Modulation Cycle of ENSO Intensity. *J. Climate*, 22, 1718-1735.

Talley, L. D., Min, D.-H., Lobanov, V. B., Luchin, V. A., Pnomarev, V. I., Salyuk, A. N., Shcherbina, A., Tishchenko, P. Y., Zhabin, I., 2006. Japan/East Sea water masses and their relation to the sea's circulation. *Oceanography* 19, 32-49.

Teague W.J., Jacobs, G.A., Perkins, H.T. and Book J.W., 2002, Low-frequency current observations in the Korea/Tsushima Strait, *J. Phys. Oceanogr*., 32, 1621-1641.

Tseng, Y. H., Jan S., Dietrich, D. E., Lin, I.-I., Chang Y. T., Tang, T. Y., 2010a. Modeled oceanic response and sea surface cooling to Typhoon Kai-Tak. *Terr. Atmos. Ocean. Sci*. 21, 85-98.

Tseng, Y.H., Chiang, C.P., Jan S., Dietrich, D. E., 2010b. Validation of the Kuroshio current system in the dual-grids Pacific ocean model framework (submitted).

Tseng, Y. H., Breaker, L. C., Chang. E. T.-Y., 2010c. Sea level variations in the regional seas around Taiwan. *J. Oceanogr*., 66, 27-39.

Vimont, D., Battisti, D., Hirst, A., 2003, The seasonal footprinting mechanism in the Pacific: Implications for ENSO, *J. Climate*, 16, 2668-2675.

Wetherill, G.B., Brown, D.W., 1991. Statistical Process Control, Theory and Practice, Chapman & Hall, London.

Wu, Z., Huang, N. E., 2008. Ensemble Empirical Mode Decomposition: a noise-assisted data analysis method. *Advances in Adaptive Data Analysis*. 1, 1-41.

Yasunari, T.,1990., Impact of Indian monsoon on the coupled atmosphere/ocean system in the tropical Pacific. *Meteorol. Atmos. Phys.*, 44, 29-41.

Yeh, S.-W., Kirtman, B.P., 2005. Pacific decadal variability and decadal ENSO amplitude modulation. *J. Geophys. Res. Lett.,* 32, L05703, doi:10.1029/2005GL021731.

Yoon, J.H.,1982. Numerical experiment on the circulation in the Japan Sea. III. Mechanism of the nearshore branch of the Tsushima Current. *J. Oceanogr. Soc. Japan,* 38, 125-130.

Youn, Y.-H., 2005. The climate variabilities of air temperature around the Korean Peninsula. *Adv. Atmos. Sci.*, 22, 575-584.

Zhang C.I., Yoon, S.C., Lee, J.B., 2007, Effects of the 1988/89 climatic regime shift on the structure and function of the southerwestern Japan/East Sea ecosystemm, *J. Marine. Syst.*, 67, 225-235.

Zhang et al. (2000), Climatic regime shifts and their impacts on marine ecosystem and fisheries resources in Korean waters, *Prog. Oceanogr.,* 47: 171-190.

Figure Captions

Figure 1a. Study area map. The three major basins are the Yamato Basin (YB), the Japan Basin (JB), and the Ulleung Basin (UB). The four main current systems are the Tsushima Warm Current (TWC), the East Korean Warm Current (EKWC), North Korean Cold Current (NKCC), and the Liman Current. The location of the subpolar front is adopted from Dorman et al's Figure 1 (2005).

Figure 2a. Summer (May-August) averaged surface pressure and velocity vector in the EJS, East China Sea (ECS), and Western North Pacific.

Figure 2b. Winter (November- February) averaged surface pressure and velocity vector in the EJS, East China Sea (ECS), and Western North Pacific.

Figure 3. 2-D daily SST (year-month diagram) from 1966 to 2004 for stations 3, 6, and 10, respectively.

Figure 4. Cross-Correlation Function (CFC) between Stations 3 and 10.

Figure 5. Variances of each EEMD mode on the first panel and EEMD modes C1 to C9 and EEMD residual from the second to the eleventh panel for station 3.

Figure 6. Variances of each EEMD mode on the first panel and EEMD modes C1 to C9 and EEMD residual from the second to the eleventh panel for station 6.

Figure 7. Variances of each EEMD mode on the first panel and EEMD modes C1 to C9 and EEMD residual from the second to the eleventh panel for station 10.

Figure 8. Cumulative sums (CUSUMs) for Scripps Pier, off southern California (8a), and Koko Head, off Oahu, Hawaii (8b), and all 3 stations (8c). Expanding means for 1976-77 regime shift off S. Korea for stations 3, 6, and 10 (3d), respectively.

Figure 9. The slopes of the long-term linear trends are shown for each month for stations 3, 6 and 10 by the lightest lines. For Station 3 (blue), stars are shown for each month, for Station 6 (green), circles are used, and for Station 10, plus signs are used. To reduce the month-to-month variability, the monthly values have been smoothed slightly and are shown by the solid darker lines. The horizontal dashed lines indicate the global mean values in each case, showing that, overall, the warming is greatest at Station 6 (~+0.054°C/yr), followed by Station 3 (~+0.05 °C/yr), and then Station 10(~+0.039 °C/yr) .

Figure 10. Mean Annual Cycles (MACs) for Stations 3, (blue), 6 (green), and 10 (red) are shown in the upper panel. Smoothed versions of the MACs are shown as well by the darker lines. The black box highlights the period during the summer when coastal upwelling occurs along the coast of South Korea. The lower panel shows this region in greater detail.

Figure 11. Linear slopes with selected EEMD mode withheld (11a) and percentage of contribution to warming with selected EEMD modes withheld (11b).

Figure 12. Time series comparison between Multivariate ENSO Index (MEI) (a) and SSTA for stations 3 (b), 6(c), and 10(d), respectively.

Figure 13a. Time series comparison between monthly mean NPGO and SSTA at each station.
Figure 13b. Time series comparison between mode C7 from an EEMD and the NPGO index at each station.
.

Figure 14. Linear regression, residual, and LOESS on the weekly mean SSTA for stations 3, 6, and 10, respectively.

Figure 15: Seasonal SST differences observed by AVHRR between 2007 and 1982.

Table Captions

Table 1. Statistics obtained from the daily raw SST data.

Table 2. Standard deviations of monthly SSTs (°C) for linear trends for Stations 3 (top), 6 (middle) and 10 (bottom).

Table 3. Statistics obtained from the Mean Annual Cycle (MAC).

Table 4. Variance of each EEMD mode for sea surface temperature with and without the MAC.

Figure 1
Click here to download high resolution image

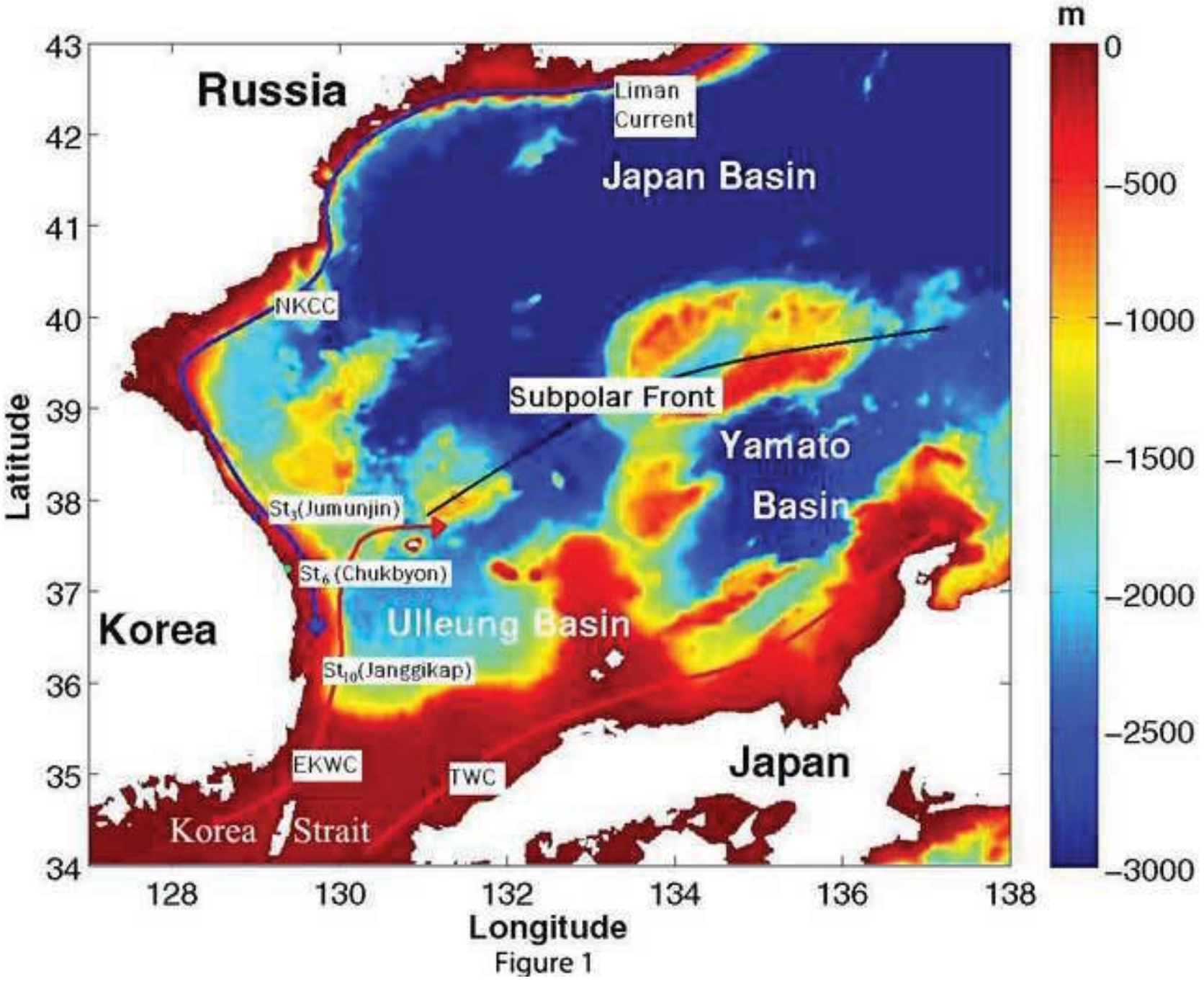

Figure 1

Figure 2a
Click here to download high resolution image

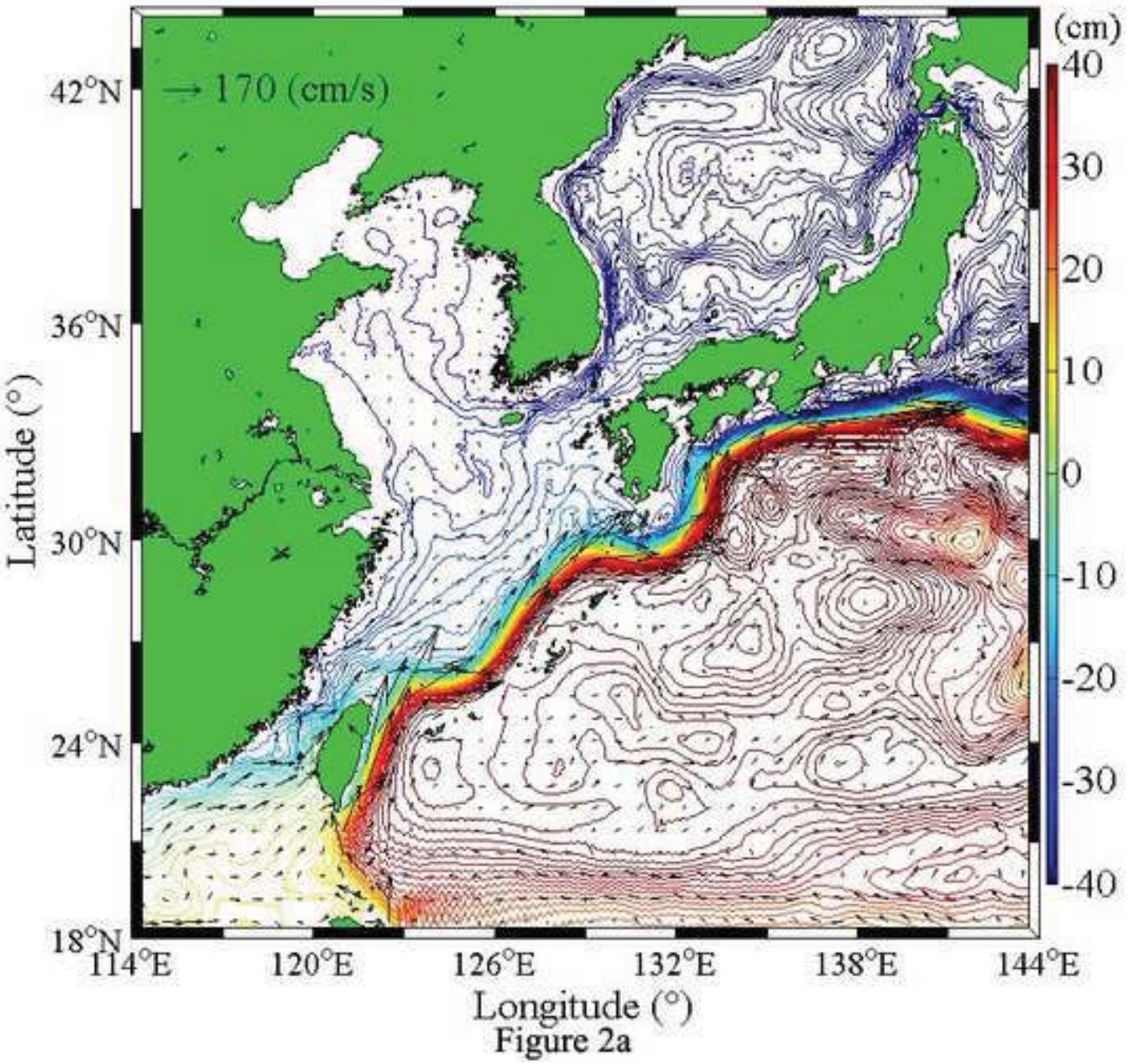

Figure 2a

Figure 2b
Click here to download high resolution image

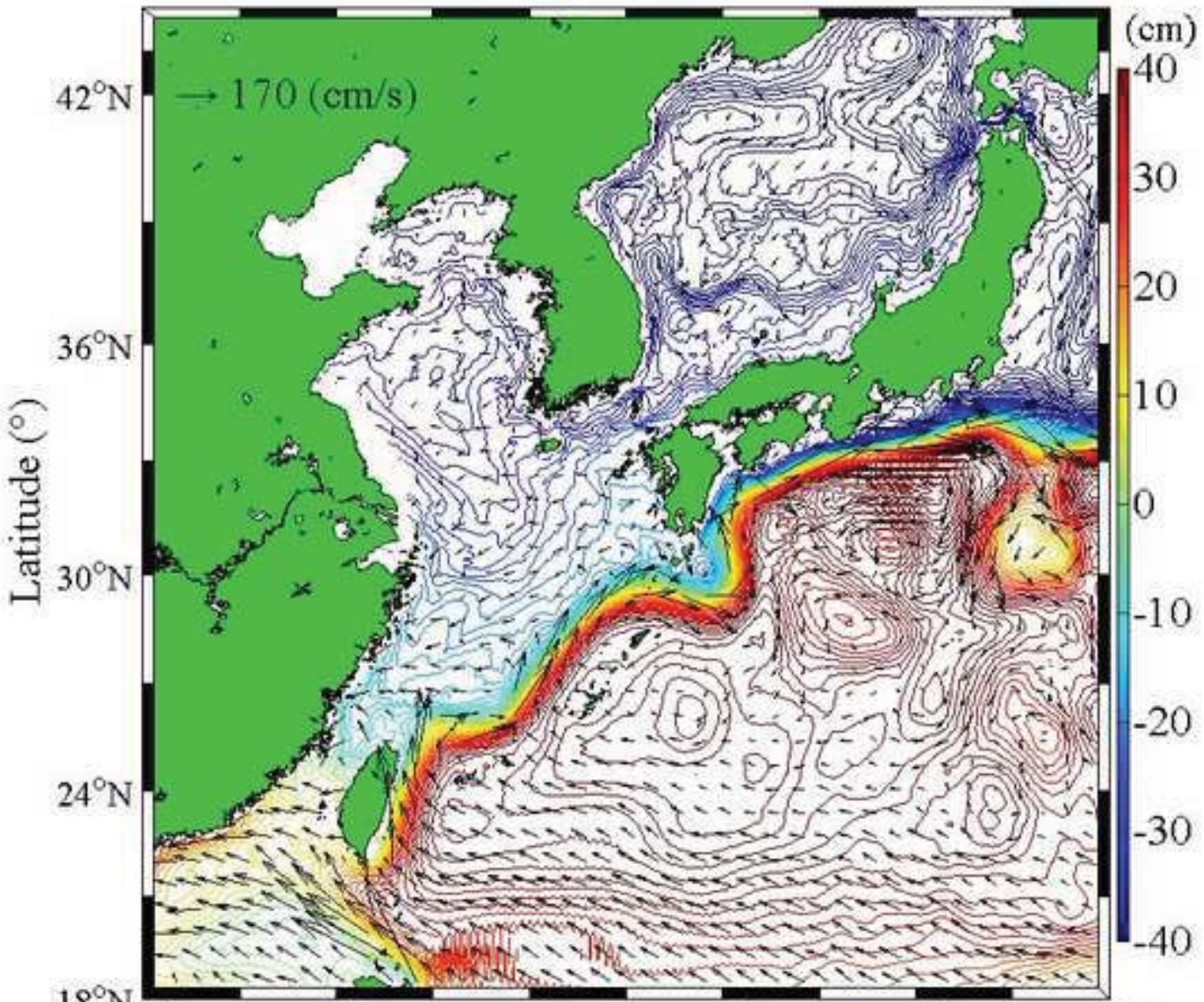

Figure 2b

Figure 3
Click here to download high resolution image

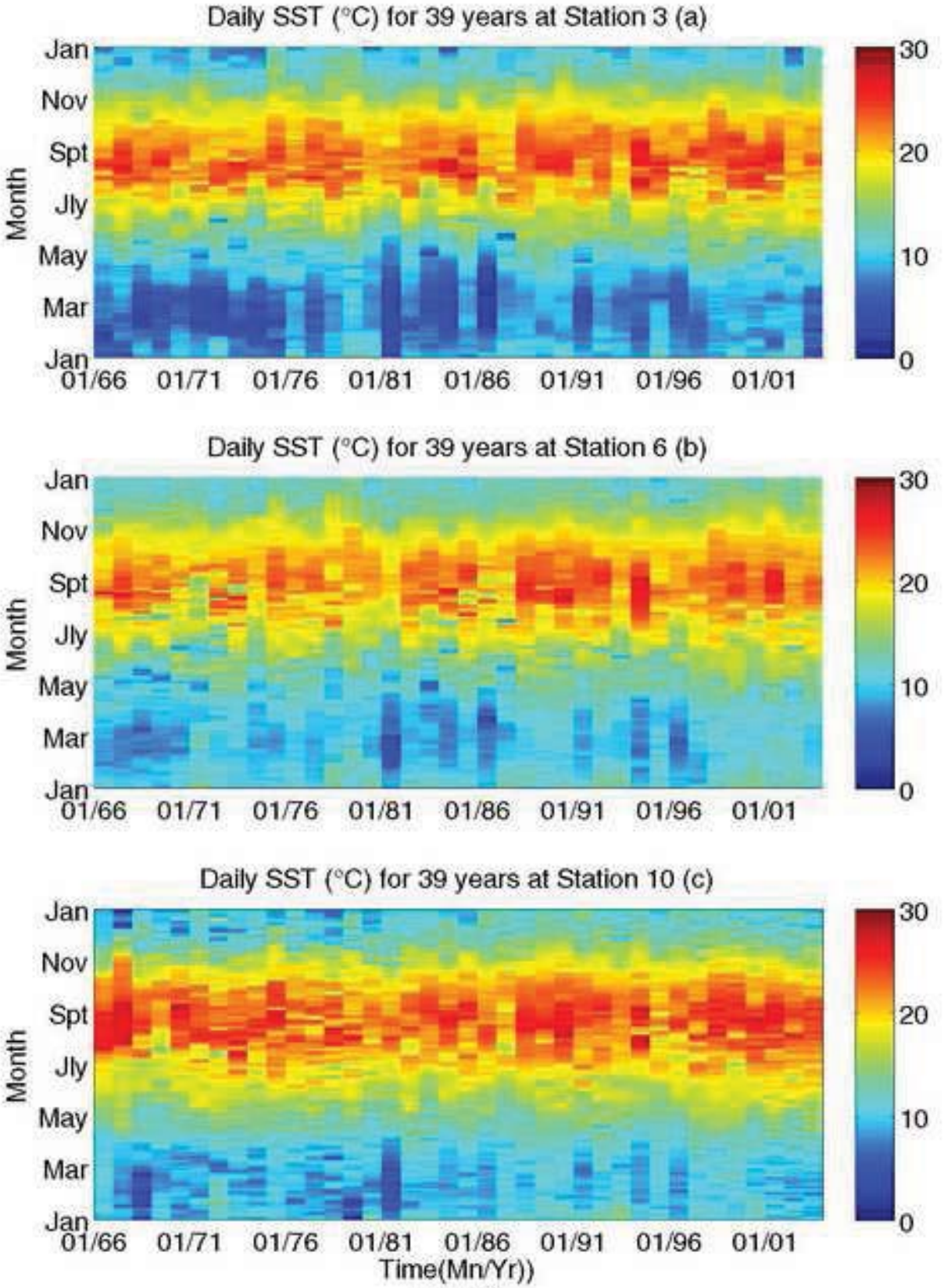

Figure 3

Figure 4
Click here to download high resolution image

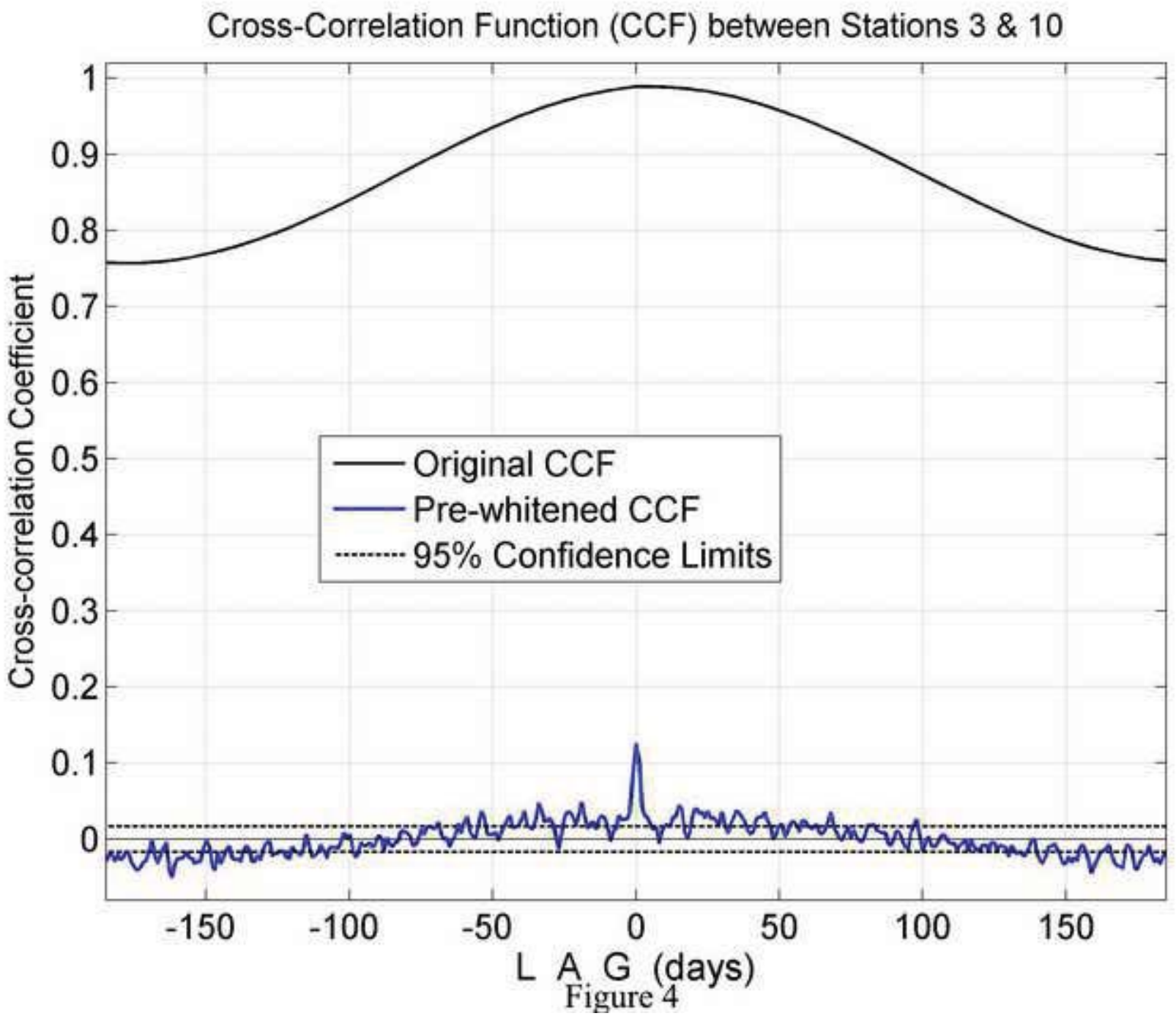

Figure 4

Figure 5
Click here to download high resolution image

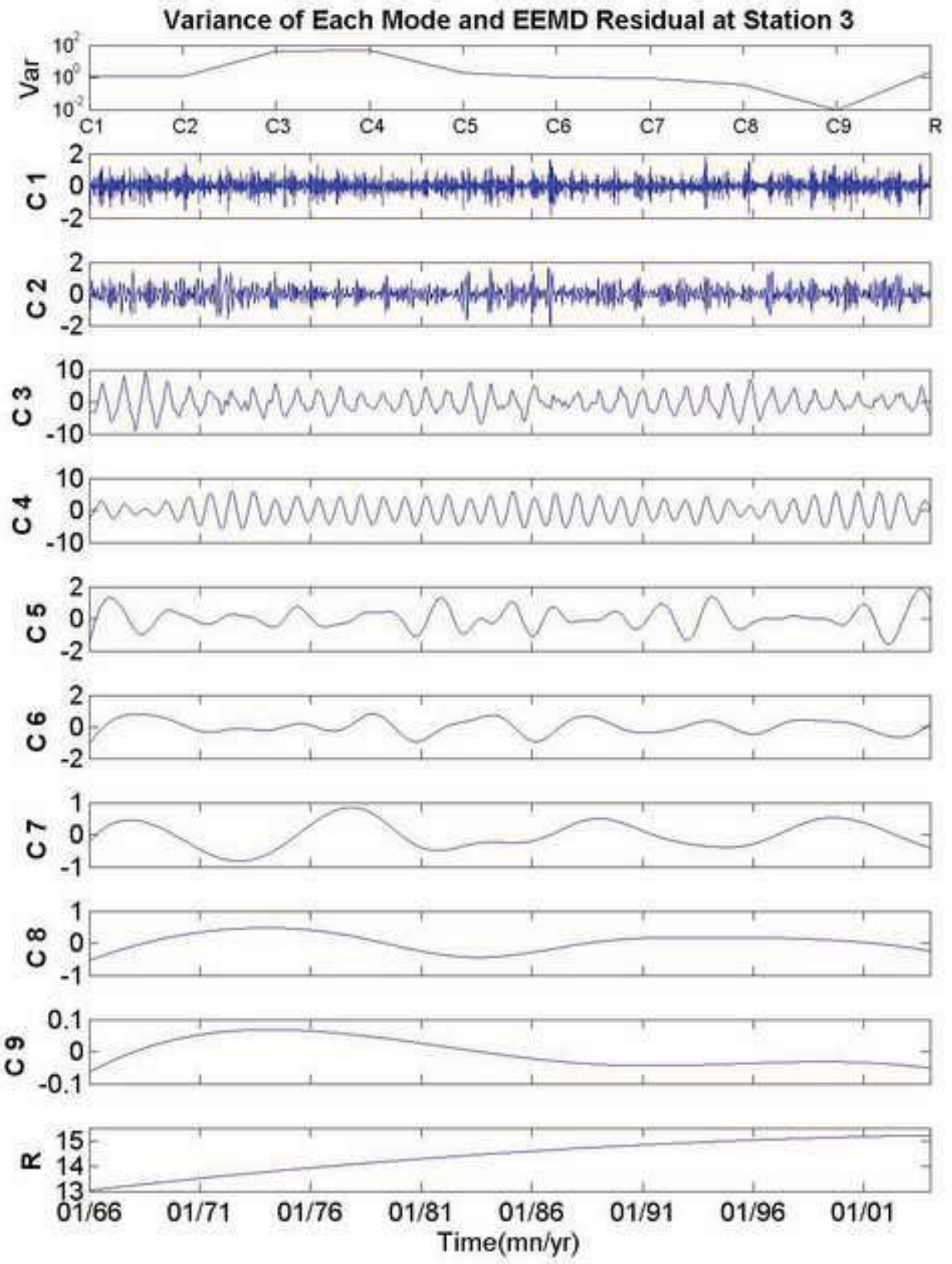

Figure 5

Figure 6
Click here to download high resolution image

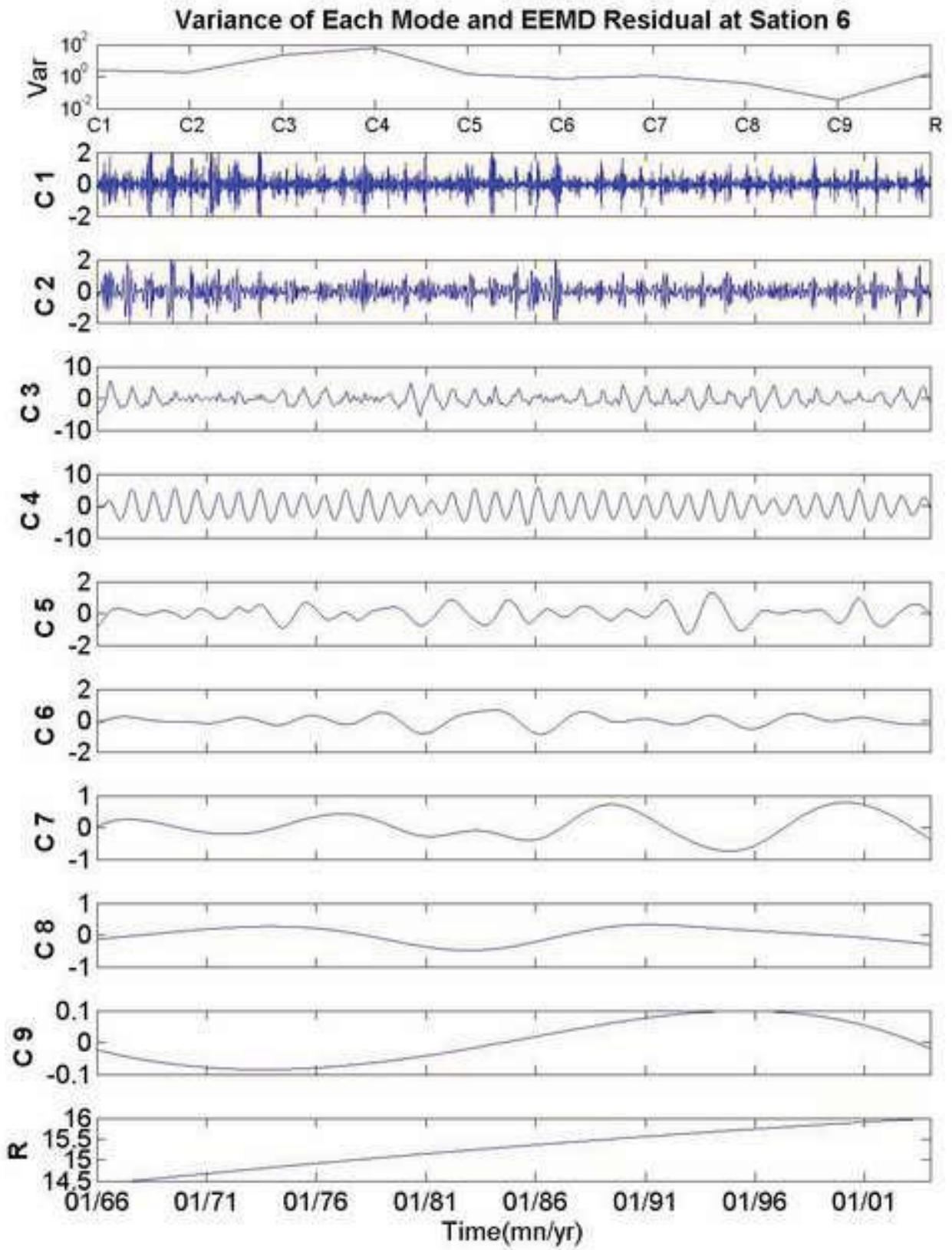

Figure 6

Figure 7
Click here to download high resolution image

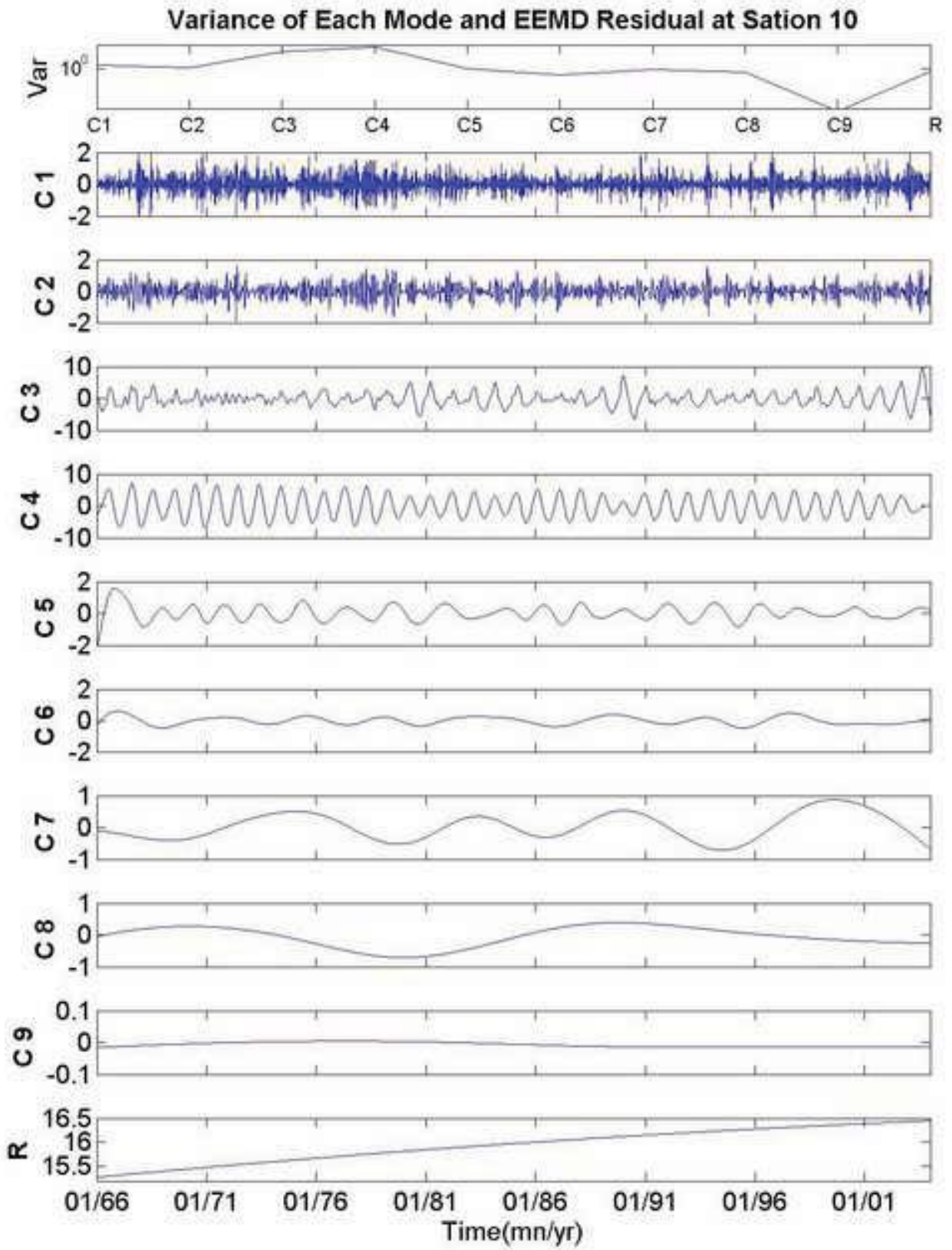

Figure 7

Figure 8
Click here to download high resolution image

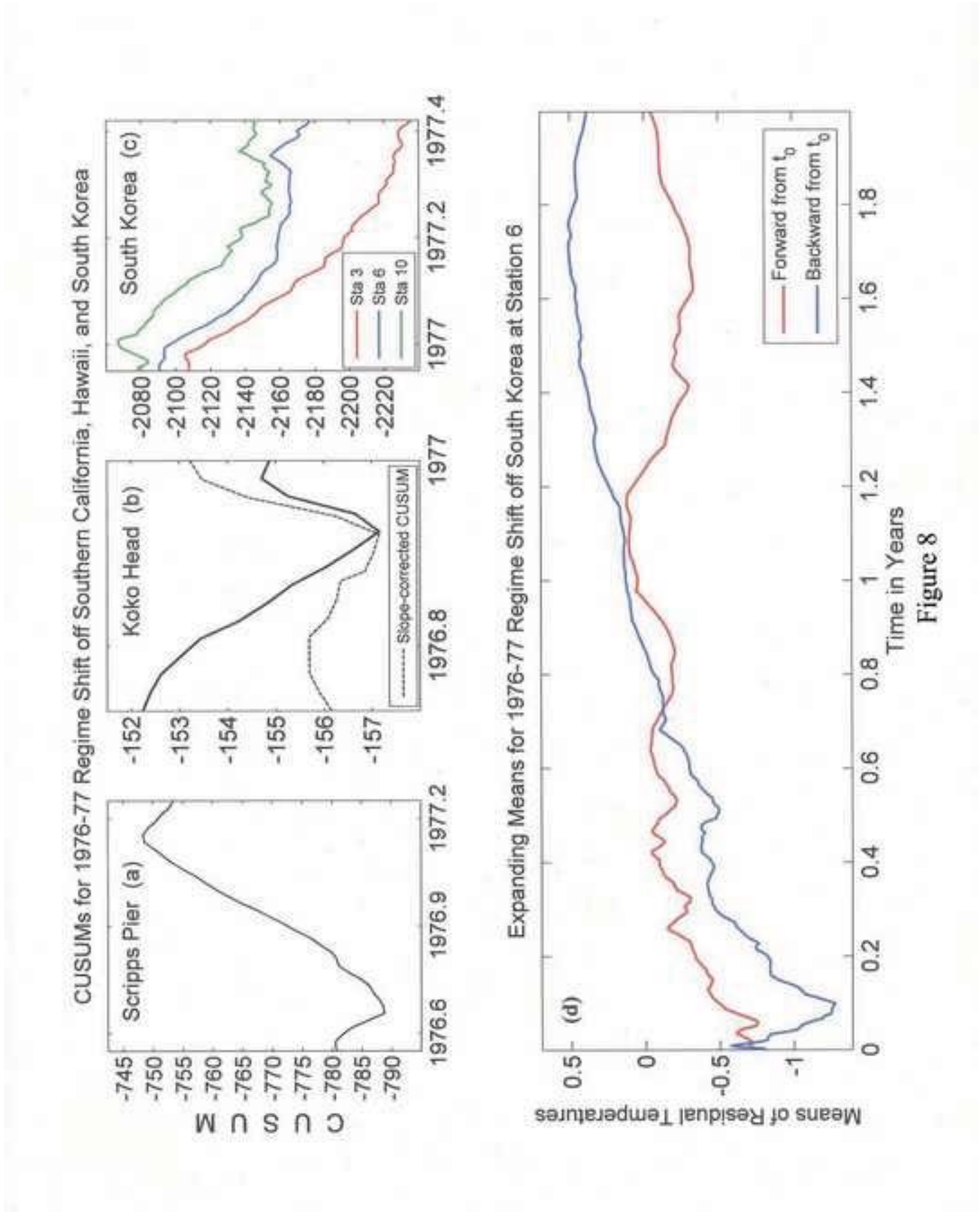

Figure 8

Figure 9
Click here to download high resolution image

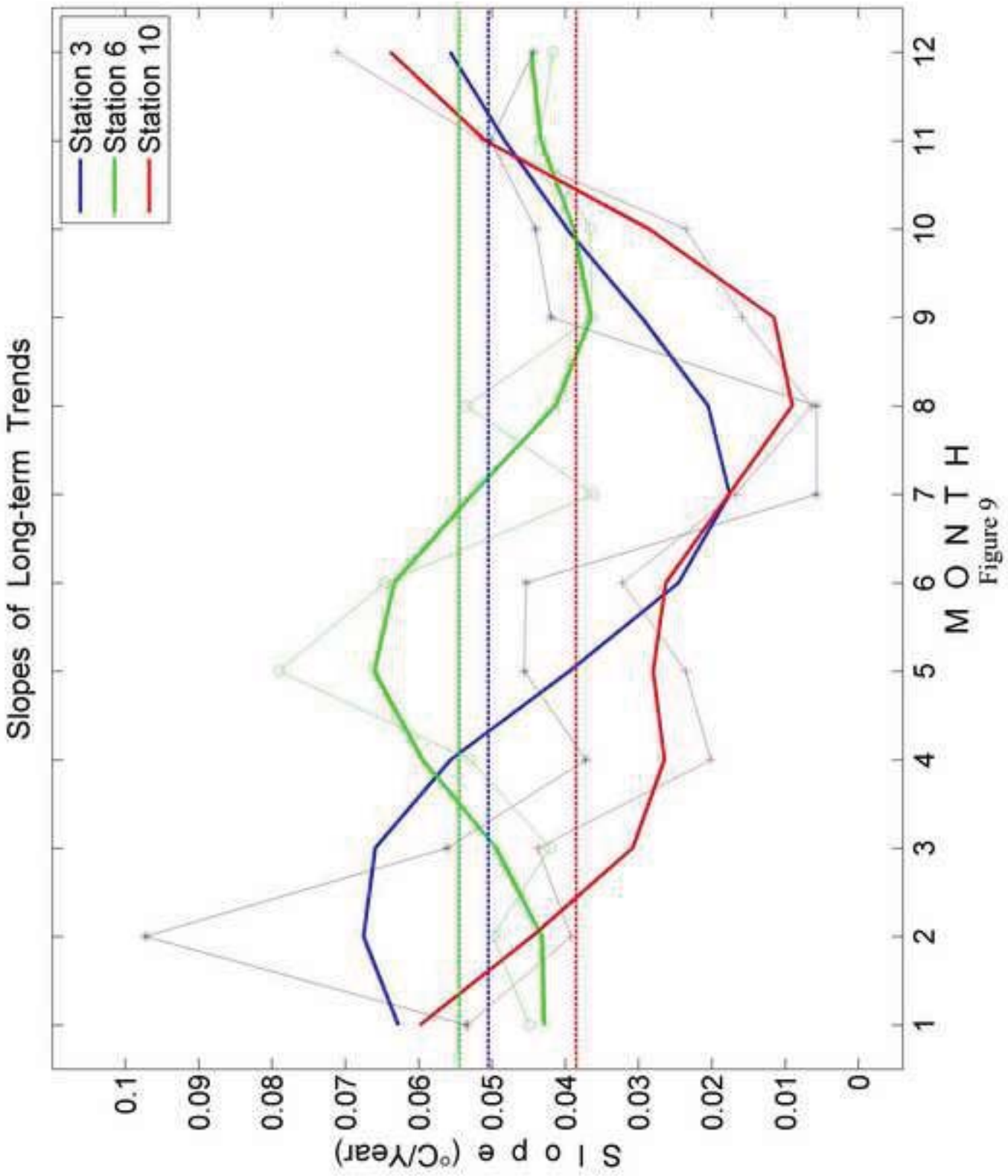

Figure 9

Figure 10
Click here to download high resolution image

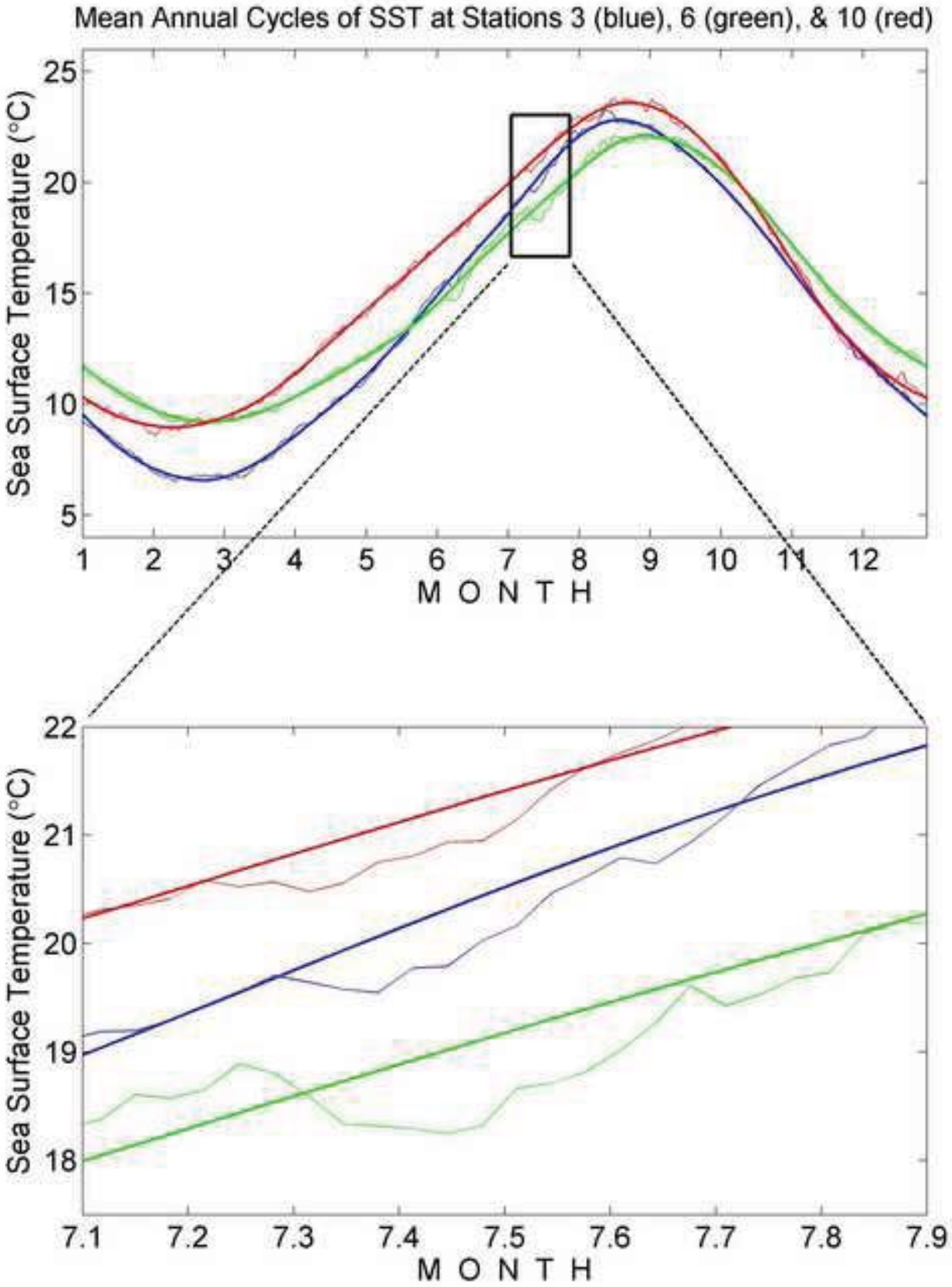

Figure 10

Figure 11a
Click here to download high resolution image

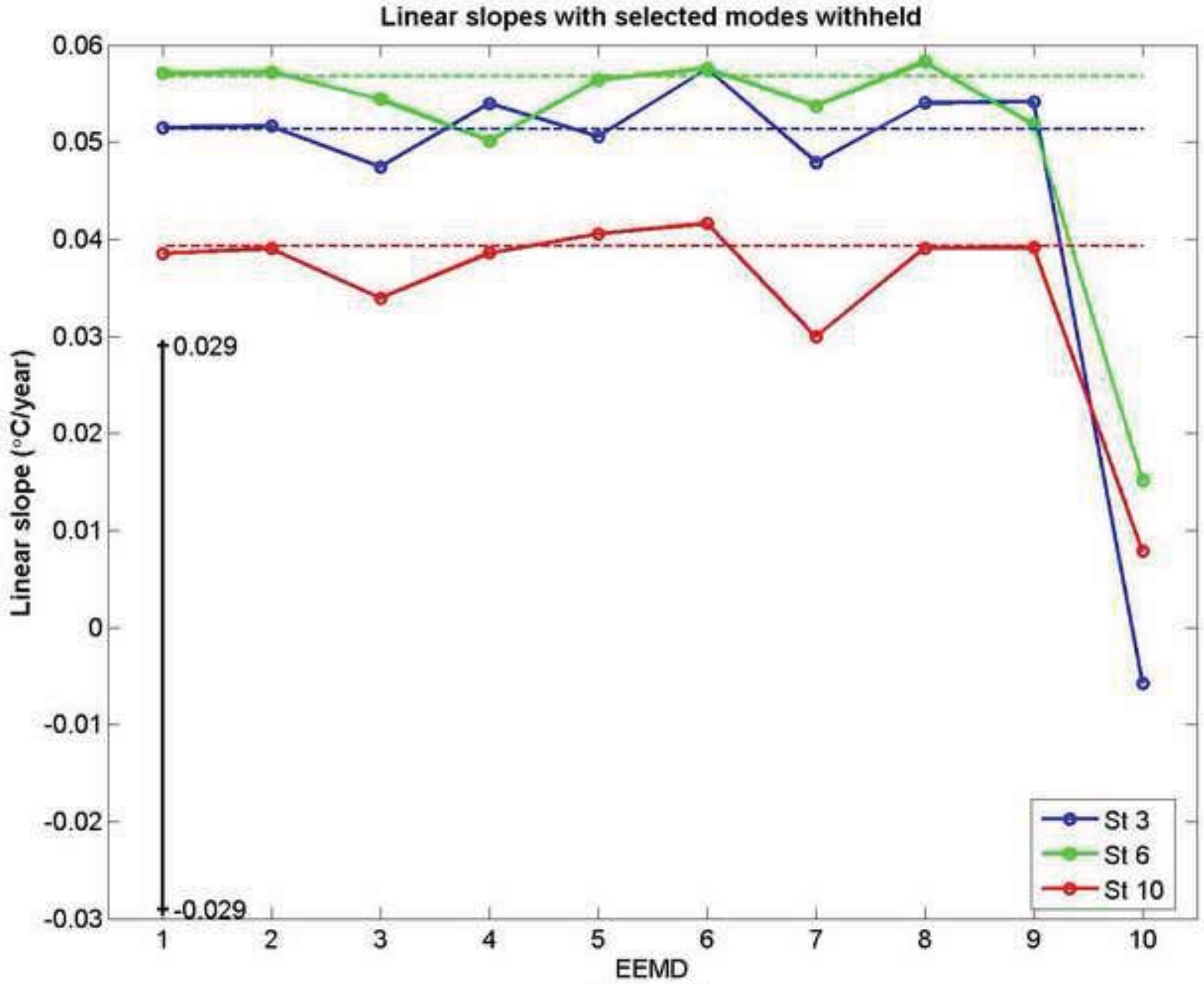

Figure 11a

Figure 11b
Click here to download high resolution image

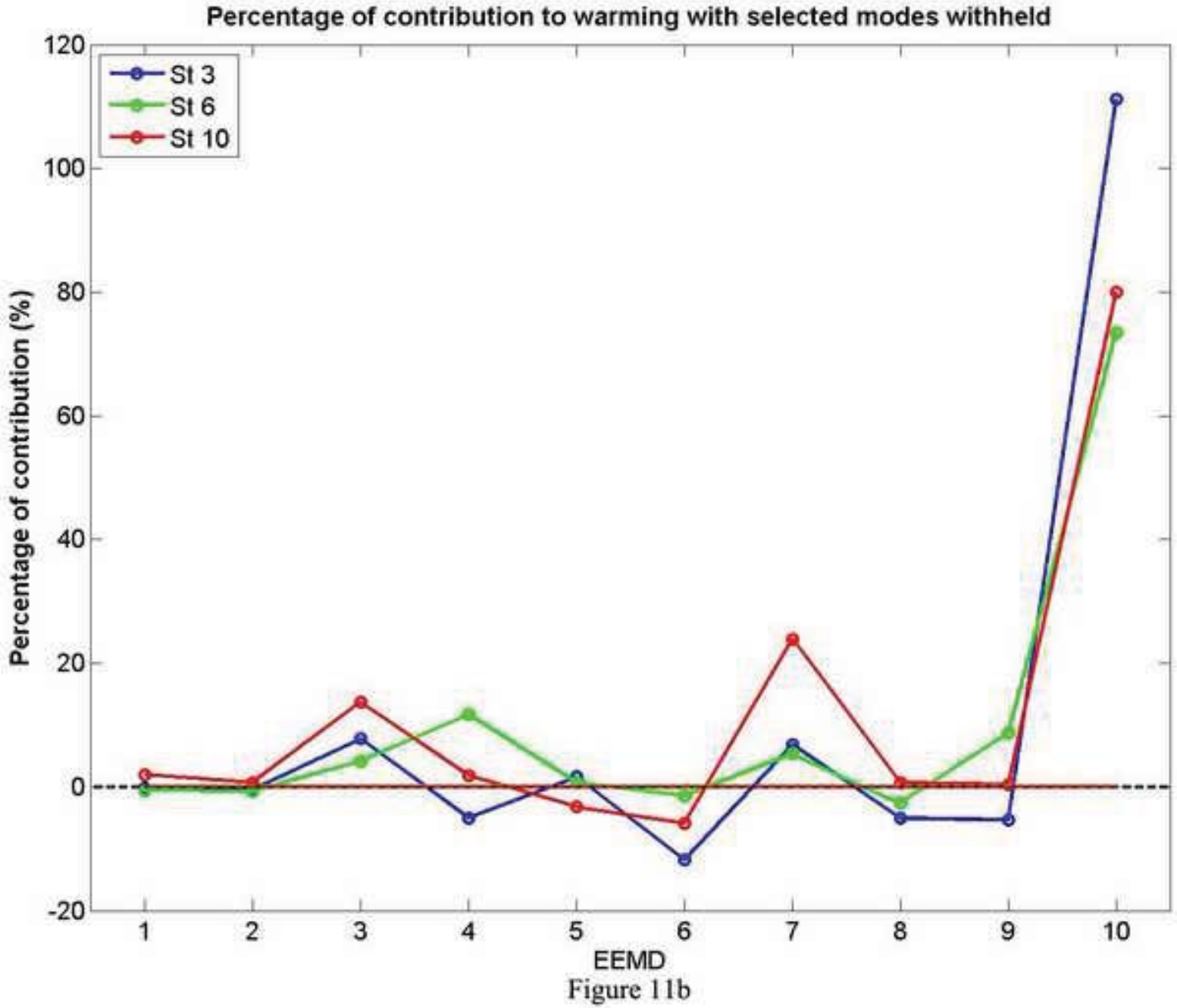

Figure 11b

Figure 12
Click here to download high resolution image

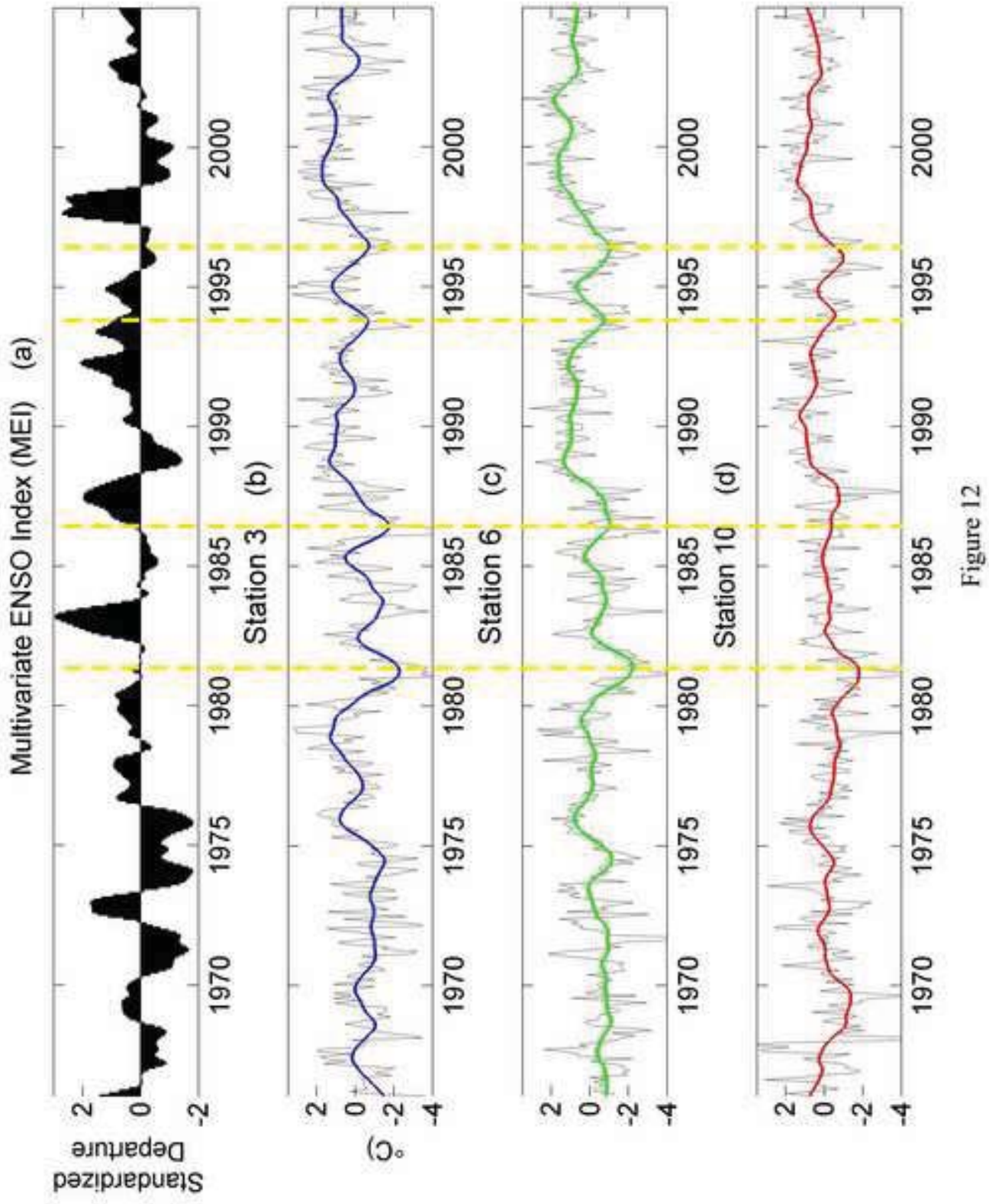

Figure 12

Figure 13a
Click here to download high resolution image

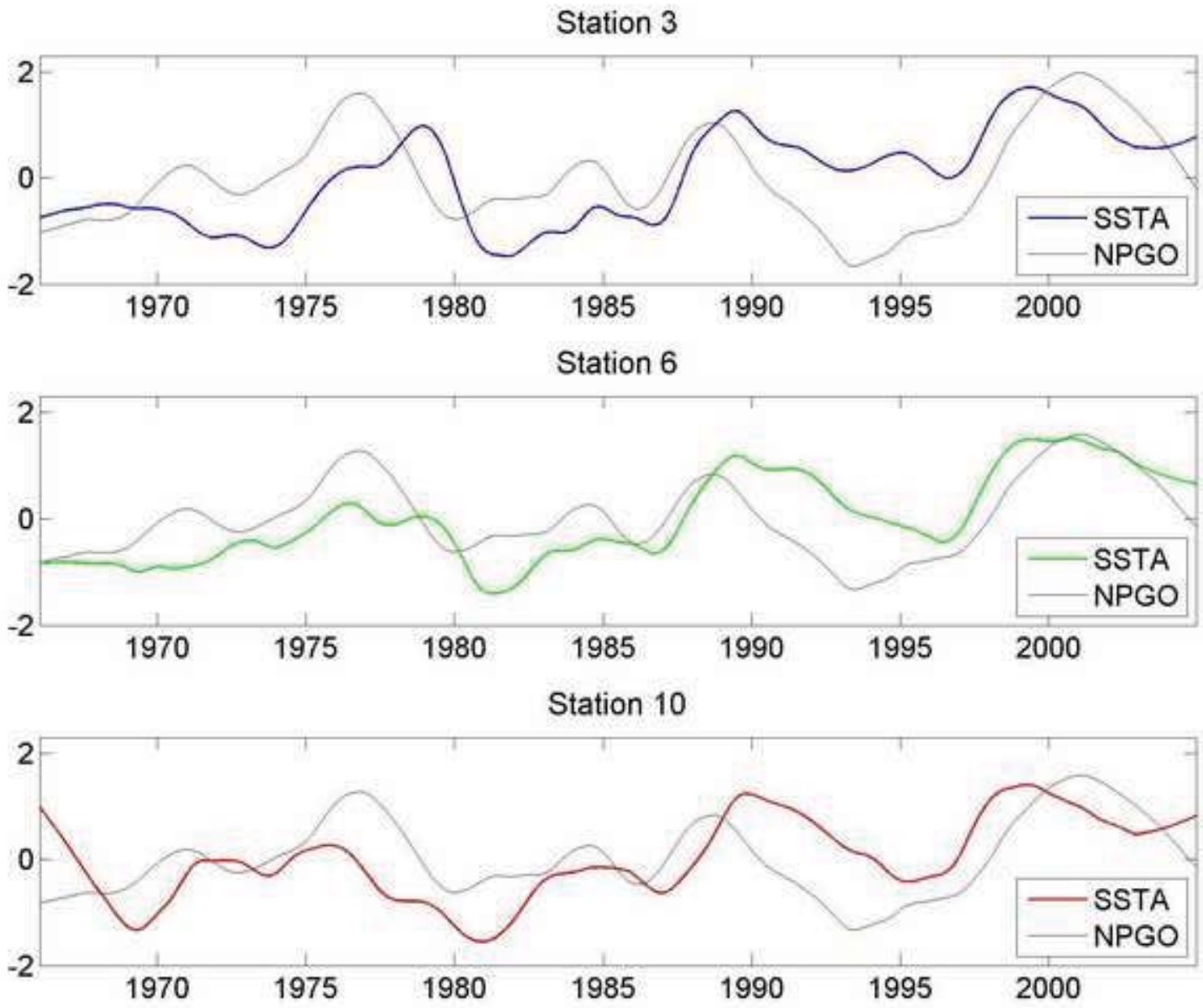

Figure 13a

Figure 13b
Click here to download high resolution image

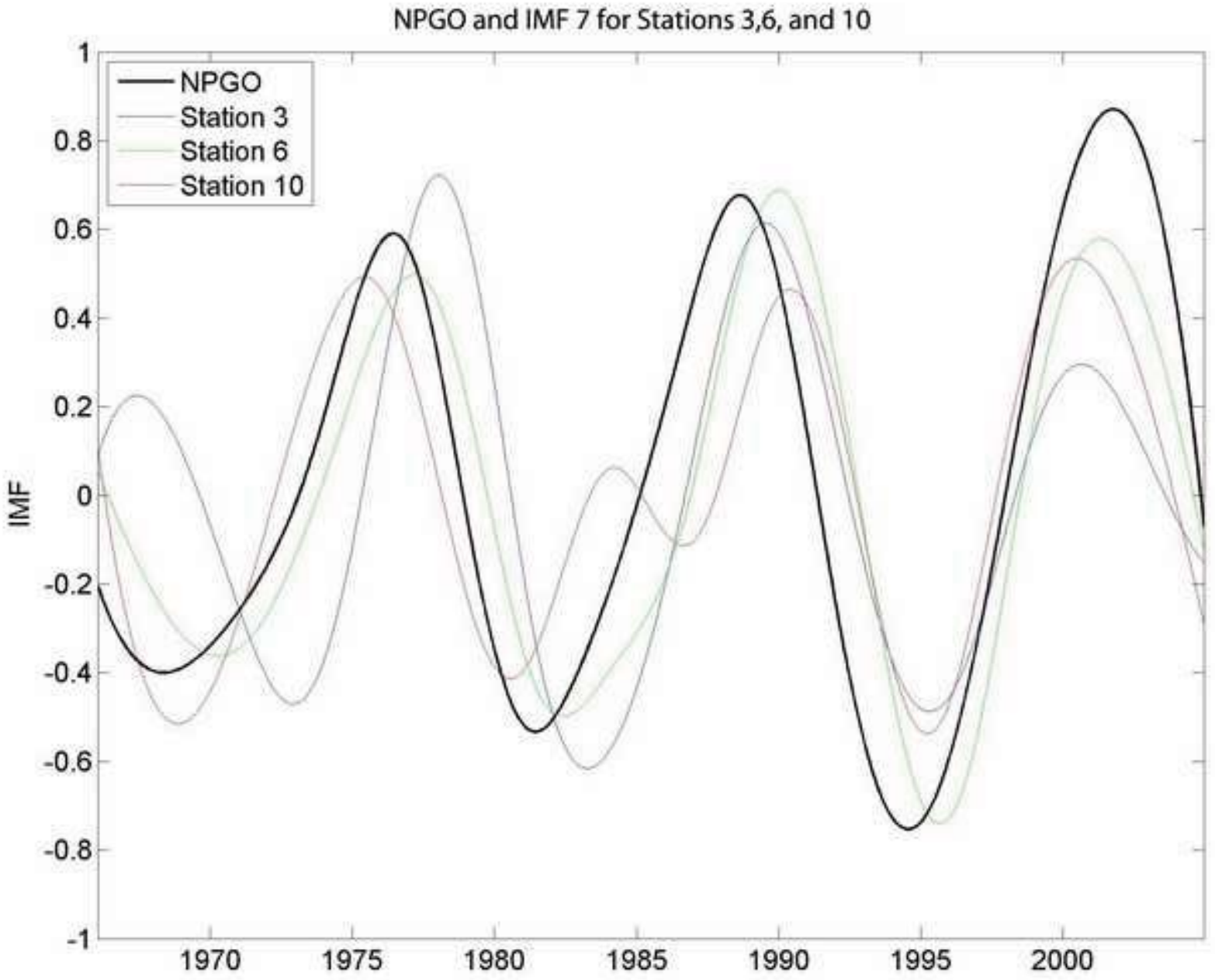

Figure 13b

Figure 14
Click here to download high resolution image

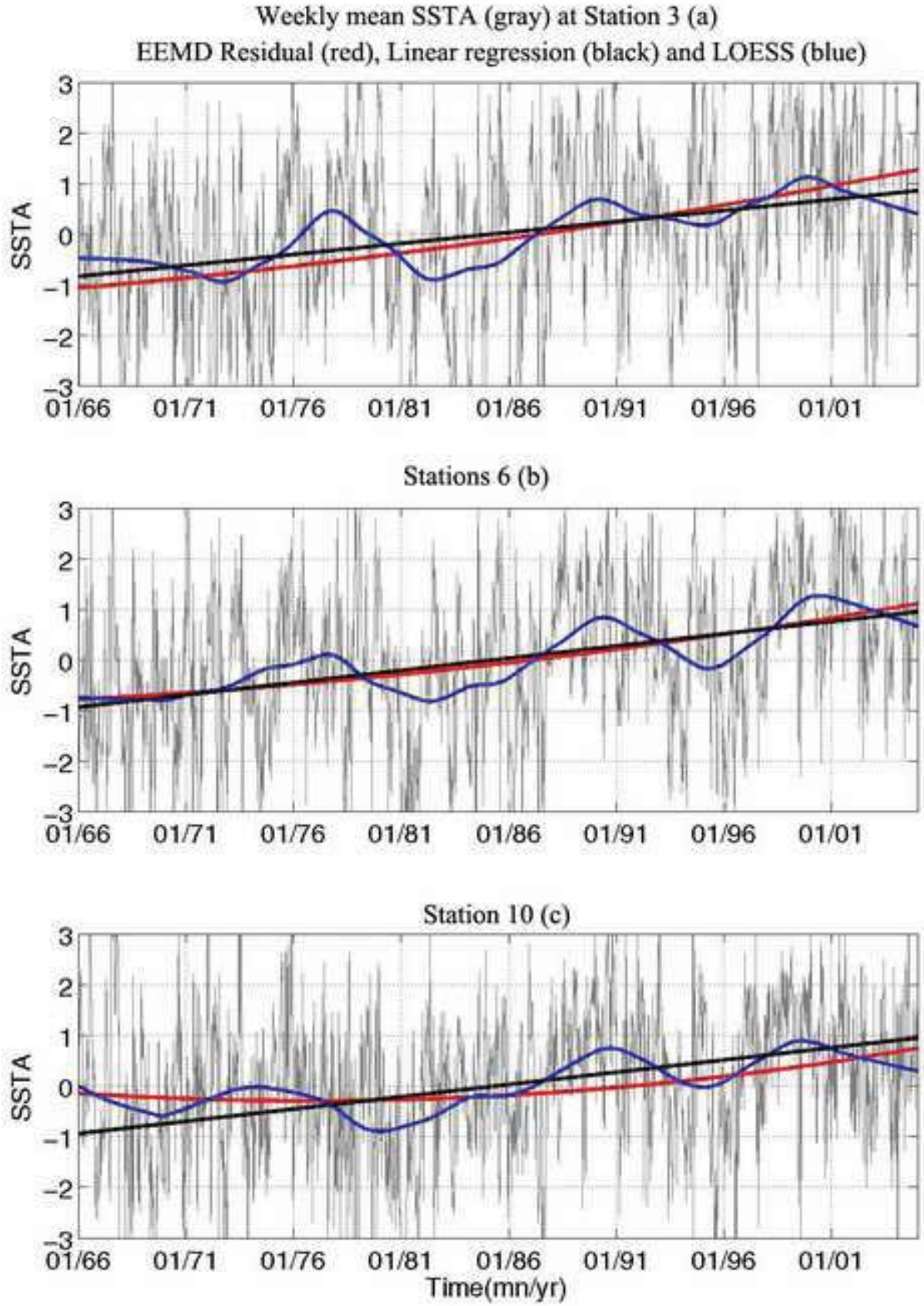

Figure 14

Figure 15
Click here to download high resolution image

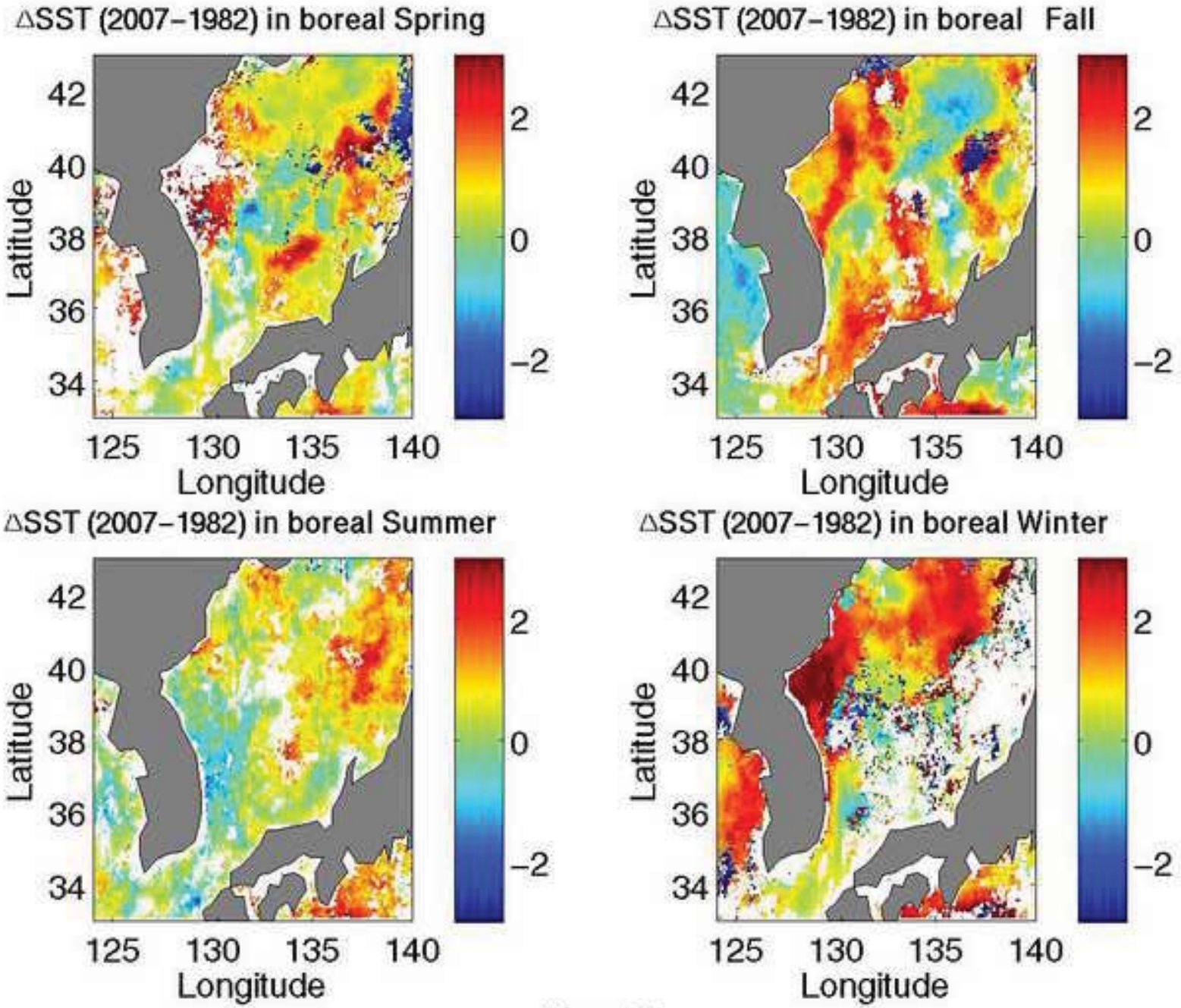

Figure 15

Table
Click here to download Table: Tables.doc

Table 1.

Station/ Statistic	Mean T (°C)	STD (°C)	Variance ($°C^2$)	Skewness	Max T (°C)	Min T (°C)	Range (°C)
3	14.09	5.77	33.29/33.61*	0.090	27.10	1.50	25.60
6	14.95	4.72	22.16/22.22*	0.260	27.50	2.80	24.70
10	15.58	5.34	28.47/28.91*	0.170	28.10	1.20	26.90

* Variances before applying a median filter

Table 2.

	1	2	3	4	5	6	7	8	9	10	11	12
St 3	1.88	2.21	1.93	1.61	1.54	1.39	1.56	1.32	1.17	0.95	1.09	1.50
St 6	1.38	1.57	1.37	1.28	1.60	1.65	1.37	1.83	1.30	0.95	1.13	1.05
St 10	1.68	1.44	1.11	0.78	1.06	1.16	1.43	1.54	1.21	1.17	1.25	1.52

Table 3.

Station/Statistic	Mean Temperature (°C)	Maximum Temperature/ Month (°C)	Minimum Temperature/ Month (°C)	Temperature Range (°C)
3	14.09	23.29 (Aug)	6.53 (Feb)	16.76
6	14.95	22.17 (Aug)	9.17 (Feb)	13.00
10	15.58	23.80 (Aug)	8.57 (Feb)	15.23

Table 4.

	SST with MAC			**SST without MAC**		
	St 3	**St 6**	**St 10**	**St 3**	**St 6**	**St 10**
C1	1.1707	2.3758	1.9930	0.2248	0.3181	0.3567
C2	1.1231	1.9159	1.1705	0.2156	0.2565	0.2095
C3	43.1473	23.5084	26.2220	8.2845	3.1479	4.6934
C4	48.1524	66.7353	67.0066	9.2456	8.9361	11.9932
C5	2.0300	1.5582	1.1119	0.3898	0.2086	0.1990
C6	0.9989	0.7844	0.3414	0.1918	0.1050	0.0611
C7	0.8814	1.1068	0.9420	0.1692	0.1482	0.1686
C8	0.3563	0.4033	0.5653	0.0684	0.0540	0.1012
C9	0.0090	0.0331	0.0003	0.0017	0.0044	0.0001
R	2.1308	1.5789	0.6469	0.4091	0.2114	0.1158